



Trapping Majorana zero modes in vortices of magnetic texture crystals coupled to nodal superconductors

Daniel Steffensen ¹, Brian M. Andersen,¹ and Panagiotis Kotetes ^{2,*}

¹Niels Bohr Institute, University of Copenhagen, Jagtvej 128, DK-2200 Copenhagen, Denmark

²CAS Key Laboratory of Theoretical Physics, Institute of Theoretical Physics, Chinese Academy of Sciences, Beijing 100190, China



(Received 2 September 2020; revised 24 October 2021; accepted 26 October 2021; published 4 November 2021)

We propose a mechanism for opening a full bulk energy gap and inducing vortex Majorana zero modes (MZMs) in nodal superconductors (SCs). We show that this becomes possible by coupling the nodal SC of interest to a magnetic texture crystal. The latter consists of superpositions of magnetic textures which repeat periodically in space according to suitable wave vectors that enable spin-flip scattering between all pairs of nodes of the SC, and thus open a full gap in its bulk energy spectrum. In this event, MZMs can be trapped in spin or shift vortices introduced in the magnetic texture crystal. Our approach is generic and applies to nodal SCs of spin-singlet, -triplet, or -mixed type of pairing. Therefore it promises to find application in a variety of nodal SCs, where the magnetic textures appear either spontaneously due to electron-electron interactions or are imposed by nanomagnets or become induced by coupling to a lattice of localized magnetic moments.

DOI: [10.1103/PhysRevB.104.174502](https://doi.org/10.1103/PhysRevB.104.174502)

I. INTRODUCTION

The experimental study of bound states in superconductors (SCs) has recently witnessed a reheated interest. This came after a series of pioneering theory proposals which designated a plethora of pathways to induce non-Abelian anyons in both intrinsic [1–6] and engineered [7–14] topological SCs. The so-called Majorana zero modes [15,16] (MZMs) are so far the most sought-after excitations of this genre, since they constitute the simplest type of non-Abelian anyons. MZMs are charge-neutral, spatially localized, pinned to zero energy, and enjoy a topological protection. In addition, they adhere to Ising exchange statistics, which open perspectives for fault-tolerant quantum computing [17–19]. The charge neutrality of MZMs brings SCs forward as ideal candidates to look for them, since their quasiparticle excitations arise from hybridized electrons and holes [20–28]. Experimental fingerprints that can be associated with MZMs have been already captured in a variety of experimental platforms, these including nanowire [29–37], topological insulator [38–41], magnetic adatom [42–49], and FeTeSe [50–54] systems.

It has been theoretically demonstrated that MZMs can be trapped at various types of 0D defects [1–7,55–60]. About three decades ago, it was theoretically shown by Read and Green [1], and by Volovik [2] in parallel, that a vortex induced in a chiral $p_x + ip_y$ SC traps a single MZM. More recently, Fu and Kane [7] proposed that a single MZM appears in a vortex of a conventional SC in proximity to the helical surface states of a 3D time-reversal (TR) invariant topological insulator. However, the vortex defects involved, need not to be introduced in the superconducting order parameter. Indeed, MZMs are also accessible if vortex defects are introduced in the phase

of another complex field or the angle of a two-component vector entering the Hamiltonian. For instance, MZMs have already been predicted to emerge in vortices of the complex order parameter of superfluid [55] and axion-string [61] condensates, as well as in the angle of a two-component spin-orbit coupling (SOC) vector field [62]. Notably, the scenario of a SOC vortex has been recently invoked as a possible mechanism to reconcile the experimental observations of a pair of MZMs in a platform of magnetic adatoms deposited on the surface of a conventional SC [48].

An additional crucial feature that a MZM platform is required to possess in order for its arising MZMs to be robust and long-lived, is to be characterized by a fully gapped bulk energy spectrum. In order to meet this stringent requirement, the vast majority of the abovementioned proposals have relied on the presence of a gapful pairing gap, i.e., of the s - and $p_x + ip_y$ types. Concomitantly, this constraint has also almost exclusively discouraged the pursuit of vortex MZMs in an equally abundant class of SCs, namely the nodal SCs [63]. Obviously, what hinders nodal SCs from joining the MZM pursuit at full speed, is that the following pressing question has remained so far unanswered, i.e., what is the suitable physical mechanism that gaps out the nodes of the nodal SC and simultaneously enables non trivial topological phases and vortex MZMs in particular.

In this paper, we show that MZMs become accessible in nodal SCs which are under the influence of magnetic texture crystals (MTCs). The MTC is exchange-coupled to the spin of the electrons of the nodal SC and can be either driven by an attractive interaction in the magnetic channel, or, imposed externally to the system. MTCs recently got in the spotlight of both theoretical [64–85] and experimental [27,36,44,47] studies. Here, we consider MTCs which consist of a superposition of magnetic helices and/or stripes. The n th helix/strip repeats periodically in space according to a wave vector \mathbf{Q}_n .

*kotetes@itp.ac.cn

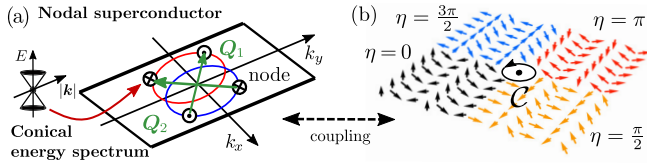


FIG. 1. (a) Typical bulk energy spectrum for a nodal superconductor discussed here. The nodes come in pairs, and the n -th pair is dictated by opposite momenta $\pm\mathbf{k}_n$ and spin projections \uparrow, \downarrow . Thus the nodes of a given pair carry the same helicity $\zeta = \pm 1$ (\otimes, \odot). The nodes are assumed to be subsequently gapped out by the presence of a magnetic helix/stripe texture with a wave vector \mathbf{Q}_n , which may either appear spontaneously due to interactions or be externally imposed. (b) Sketch of a magnetic helix crystal with a spatial profile $\mathbf{M} \sim \cos[\mathbf{Q} \cdot \mathbf{r} + \eta(\mathbf{r})]\hat{z} + \sin[\mathbf{Q} \cdot \mathbf{r} + \eta(\mathbf{r})]\hat{x}$. The wave vector is chosen as $\mathbf{Q} = (2\pi/3, 0)$. The texture additionally contains a discrete shift defect with vorticity $v_{\text{shift}} = \sum_C \Delta\eta/2\pi = 1$.

Each \mathbf{Q}_n needs to have a length comparable to $2|\mathbf{k}_n|$, so that it couples and gaps out a pair of nodes of the underlying SC at momenta $\pm\mathbf{k}_n$. In Fig. 1, we depict a representative nodal bulk energy spectrum where our theory finds application, and we additionally sketch the spatial profile of a MTC containing a shift vortex defect.

Within our proposal, MZMs can be trapped in spin or shift vortices induced in the MTC. In fact, our topological analysis proves that MZMs appear in vortices of the MTC *only* when the underlying SC is nodal. Our theory applies to generic nodal SCs with spin-singlet, -triplet or -mixed [86] pairing, thus covering a broad range of quantum materials and hybrid structures. Remarkably, for systems featuring a Rashba SOC, MZMs can be even trapped by inducing vortices in MTCs which are as mundane as magnetic stripes.

Our upcoming analysis provides a detailed study of the various topological scenarios that become possible in both 2D and 3D nodal SCs, for all the Majorana symmetry classes, i.e., BDI, D, and DIII. This is achieved by first constructing the topological invariant quantities which predict the emergence of Majorana quasiparticles in two fundamental situations, with these concerning systems belonging to class BDI in 2D and to class D in 3D. Notably, as we discuss here, nodal SCs coupled to MTCs which belong to class D harbor chiral vortex Majorana modes in 3D. Even more remarkably, we demonstrate that, despite the fact that MTCs break the standard TR symmetry (\mathcal{T}), symmetry class DIII SCs, and Majorana Kramers pair solutions are still accessible in both 2D and 3D when a generalized TR symmetry Θ with $\Theta^2 = -\mathbb{1}$ appears [68]. Such a symmetry emerges, for instance, when we consider two-band systems, with the electrons of the two bands feeling identical nonmagnetic terms, but opposite MTC terms.

The remainder of this manuscript is organized as follows. Section II contains the details of our theoretical model and sets the stage for our upcoming analysis. Section III gives an account of the various types of topological phases and Majorana excitations which become accessible. In Sec. IV, we derive a low-energy model which describes the physics stemming from the nodes of the SC. Based on this low-energy mode, we proceed in Sec. V with the construction of the topological invariant for a class BDI system in 2D, which

predicts the emergence of multiple vortex MZMs protected by chiral symmetry. Section VI presents a series of numerical investigations of BDI, D, and DIII models in 2D. In Sec. VII, we focus on 3D systems and, in particular, we construct the topological invariant for the class D case. Section VIII presents numerical results for the emergence of chiral vortex Majorana modes. Section IX gives an account of possible routes to experimentally realize our proposal, while Sec. X concludes this work with a summary and outlook.

II. MODEL HAMILTONIAN

To model the physical situations of interest in a general manner, we employ the Hamiltonian operator:

$$\hat{H} = \frac{1}{2} \int d\mathbf{r} \Psi^\dagger(\mathbf{r}) \hat{\mathcal{H}}(\hat{\mathbf{p}}, \mathbf{r}) \Psi(\mathbf{r}), \quad (1)$$

which acts in the basis defined by the Nambu spinor:

$$\Psi^\dagger(\mathbf{r}) = (\psi_\uparrow^\dagger(\mathbf{r}), \psi_\downarrow^\dagger(\mathbf{r}), \psi_\downarrow(\mathbf{r}), -\psi_\uparrow(\mathbf{r})). \quad (2)$$

Here, $\psi_{\uparrow,\downarrow}(\mathbf{r})$ annihilates an electron at position \mathbf{r} with the spin projection indicated, while $\hat{\mathbf{p}} = -i\nabla$ with $\hbar = 1$. In 3D coordinate space, we define $\mathbf{r} = (x, y, z)$, $\tan \phi = y/x$, $\cos \theta = z/r$, $r = \sqrt{\rho^2 + z^2}$ and $\rho = \sqrt{x^2 + y^2}$.

The matrix $\hat{\mathcal{H}}(\hat{\mathbf{p}}, \mathbf{r})$ defines the Bogoliubov - de Gennes (BdG) Hamiltonian operator:

$$\hat{\mathcal{H}}(\hat{\mathbf{p}}, \mathbf{r}) = \hat{\mathcal{H}}_0(\hat{\mathbf{p}}) + \sum_n \{2M_n \cos[\mathbf{Q}_n \cdot \mathbf{r} + \eta_n(\mathbf{r})] \hat{\mathbf{e}}_n \cdot \boldsymbol{\sigma} - 2M'_n \sin[\mathbf{Q}_n \cdot \mathbf{r} + \eta_n(\mathbf{r})] \hat{\mathbf{e}}'_n \cdot \boldsymbol{\sigma}\} e^{-i\omega_n(\mathbf{r})\sigma_z}, \quad (3)$$

and is represented using the $\boldsymbol{\tau}$ ($\boldsymbol{\sigma}$) Pauli matrices defined in Nambu (spin) spaces, supplemented with the respective unit matrix $\mathbb{1}_\tau$ ($\mathbb{1}_\sigma$). For simplicity, we omit writing unit matrices throughout from now on. In the above, we consider that the two contributing magnetization terms always feature orthogonal orientations in spin space, i.e., their orientation vectors satisfy $\hat{\mathbf{e}}_n \cdot \hat{\mathbf{e}}'_n = 0$ for all n .

The nonmagnetic part of the BdG Hamiltonian takes the general form:

$$\hat{\mathcal{H}}_0(\hat{\mathbf{p}}) = \tau_z[\varepsilon_s(\hat{\mathbf{p}}) + \varepsilon_t(\hat{\mathbf{p}})\sigma_z] + \tau_x[\Delta_s(\hat{\mathbf{p}}) + \Delta_t(\hat{\mathbf{p}})\sigma_z] + \tau_y[\Delta'_s(\hat{\mathbf{p}}) + \Delta'_t(\hat{\mathbf{p}})\sigma_z], \quad (4)$$

where the appearing terms satisfy the relations:

$$\varepsilon_{s,t}(-\hat{\mathbf{p}}) = \pm \varepsilon_{s,t}(\hat{\mathbf{p}}), \quad (5)$$

$$\Delta_{s,t}(-\hat{\mathbf{p}}) = \pm \Delta_{s,t}(\hat{\mathbf{p}}), \quad (6)$$

$$\Delta'_{s,t}(-\hat{\mathbf{p}}) = \pm \Delta'_{s,t}(\hat{\mathbf{p}}). \quad (7)$$

The above properties imply that $\hat{\mathcal{H}}_0(\hat{\mathbf{p}})$ is invariant under translations and z -axis spin rotations, associated with the phases $\eta_n(\mathbf{r})$ and angles $\omega_n(\mathbf{r})$, respectively. Vortices can be independently introduced in all ω_n angles and η_n phases, at the same or different positions.

For a shift [spin] vortex defect with vorticity v_{shift} [v_{spin}] we set $\eta(\mathbf{r}) = v_{\text{shift}}\phi$ [$\omega(\mathbf{r}) = v_{\text{spin}}\phi$]. In Fig. 1(b), we depict the spatial profile of a magnetic helix crystal with a discrete shift vortex. A shift vortex defect in $\eta(\mathbf{r})$ implies that this

phase shows discontinuous jumps by an integer multiple of 2π after traversing a closed path \mathcal{C} encircling the defect's core, which is identified with the region where the magnetic texture vanishes. A similar behavior emerges for $\omega(\mathbf{r})$ in the presence of a spin vortex. The above properties are reflected in the definitions of the shift ν_{shift} and spin ν_{spin} vorticities:

$$\nu_{\text{shift}} = \oint_{\mathcal{C}} \frac{d\eta}{2\pi} \in \mathbb{Z} \quad \text{and} \quad \nu_{\text{spin}} = \oint_{\mathcal{C}} \frac{d\omega}{2\pi} \in \mathbb{Z}. \quad (8)$$

III. ACCESSIBLE TOPOLOGICAL PHASES

To infer the emergence of Majorana quasiparticles in our model, we employ standard classification methods, cf Refs. [58,59]. The topological classification of the system in the presence of defects is carried out using the BdG Hamiltonian in combined momentum-coordinate space $\hat{\mathcal{H}}(\mathbf{k}, \mathbf{r})$, which is obtained by assuming that the defect builds up in a sufficiently smooth manner in space, so that the momentum $\hat{\mathbf{p}} \mapsto \mathbf{k}$ and the position \mathbf{r} appearing in $\eta(\mathbf{r})$ and $\omega(\mathbf{r})$ commute. This approach suffices to predict the appearance of MZMs but generally fails to accurately describe the complete bound state spectrum that we observe in our numerics using abrupt defects.

The relevant Majorana symmetry class, i.e., BDI, D or DIII, is inferred in the presence of the defect-containing variables. The effective classification dimension δ is obtained by the spatial dimensionality of the system d , after subtracting the dimension of the surface that can enclose the defect, i.e., here $\delta = d - 1$ since a circle \mathbb{S}^1 can enclose a vortex. To construct the topological invariants, we view ϕ as a synthetic momentum which extends the base space to (\mathbf{k}, ϕ) .

Based on the tenfold classification tables [87–89], we find the topologically-nontrivial scenarios $\{\text{BDI, D, DIII}\} \mapsto \{\mathbb{Z}, \mathbb{Z}_2, \mathbb{Z}_2\}$ in 2D, and $\{\text{D, DIII}\} \mapsto \{\mathbb{Z}, \mathbb{Z}_2\}$ in 3D. For the topological description of the cases of relevance in 2D (3D) coordinate space, it suffices to examine the structure of the class BDI (D) \mathbb{Z} topological invariant, which is identified with the winding number w_3 (2nd Chern number C_2). Here, we obtain general expressions for w_3 and C_2 , which become particularly transparent in the limit of a weak strength for the magnetization of the MTC.

IV. LOW-ENERGY MODEL HAMILTONIAN - DERIVATION

Similar to Ref. [60], which discusses MZMs trapped in superconducting vortices, also here, the outcome of the various topological invariants is tied to the local, instead of the global, \mathbf{k} -space topology of $\hat{\mathcal{H}}_0(\mathbf{k})$. Therefore, to facilitate the calculation of the various topological invariants, we rely on low-energy models obtained after expanding the original Hamiltonian about pairs of nodes with momenta $\pm\mathbf{k}_n$.

To simplify our upcoming analysis, we momentarily drop the terms $\Delta'_{s,p}(\hat{\mathbf{p}})$ from the Hamiltonian in Eq. (4), and restore them for the discussion of 3D models in Sec. VIII. Under the above simplification, the various pairs of nodes are determined by $\hat{\mathcal{H}}_0(\mathbf{k}) = \hat{0}$, which boils down to satisfying the condition:

$$\varepsilon_s(\mathbf{k}_n) \pm \sigma_z \varepsilon_t(\mathbf{k}_n) = \Delta_s(\mathbf{k}_n) \pm \sigma_z \Delta_t(\mathbf{k}_n) = \hat{0}. \quad (9)$$

Since $\{\varepsilon_t(-\mathbf{k}), \Delta_t(-\mathbf{k})\} = -\{\varepsilon_t(\mathbf{k}), \Delta_t(\mathbf{k})\}$ we find that nodes at opposite momenta $\pm\mathbf{k}_n$ carry opposite spins $\sigma_z = \pm 1$, i.e., possess the same helicity. See Fig. 1(a).

We now expand the Hamiltonian about the n th pair of nodes by setting $\mathbf{k} \approx \pm\mathbf{k}_n + \mathbf{q}$ with $|\mathbf{q}| \ll |\mathbf{k}_n|$. By introducing the ρ Pauli matrices in $\{\mathbf{k}_n, -\mathbf{k}_n\}$ nodes space, the defect-free Hamiltonian in the vicinity of $\pm\mathbf{k}_n$ reads

$$\begin{aligned} \hat{\mathcal{H}}^{(n)}(\mathbf{q}, \phi = 0) &= M_n \rho_x \hat{\mathbf{e}}_n \cdot \boldsymbol{\sigma} - M'_n \rho_y \hat{\mathbf{e}}'_n \cdot \boldsymbol{\sigma} \\ &+ \tau_z [\varepsilon_s^{(n)} + \mathbf{v}_{\varepsilon_t}^{(n)} \cdot \mathbf{q} \sigma_z] + \rho_z \tau_z [\mathbf{v}_{\varepsilon_s}^{(n)} \cdot \mathbf{q} + \varepsilon_t^{(n)} \sigma_z] \\ &+ \tau_x [\Delta_s^{(n)} + \mathbf{v}_{\Delta_t}^{(n)} \cdot \mathbf{q} \sigma_z] + \rho_z \tau_x [\mathbf{v}_{\Delta_s}^{(n)} \cdot \mathbf{q} + \Delta_t^{(n)} \sigma_z], \end{aligned} \quad (10)$$

where we used the shorthand expressions for $f = \varepsilon, \Delta$:

$$f_{s,t}^{(n)} = f_{s,t}(\mathbf{k}_n) \quad \text{and} \quad \mathbf{v}_{f,s,t}^{(n)} = \nabla_{\mathbf{k}} f_{s,t}(\mathbf{k}) \Big|_{\mathbf{k}=\mathbf{k}_n}. \quad (11)$$

The nonmagnetic part of Eq. (10), that we denote $\hat{\mathcal{H}}_0^{(n)}(\mathbf{q})$, is invariant under arbitrary ϕ -dependent shifts and spin rotations generated by the operators $\hat{\mathcal{L}}_{\text{shift}}^{(n)} = \rho_z$ and $\hat{\mathcal{L}}_{\text{spin}}^{(n)} = \sigma_z$. Thus the defects are added as follows:

$$\hat{\mathcal{H}}^{(n)}(\mathbf{q}, \phi) = e^{i\phi \hat{\mathcal{L}}^{(n)}/2} \hat{\mathcal{H}}^{(n)}(\mathbf{q}, \phi = 0) e^{-i\phi \hat{\mathcal{L}}^{(n)}/2}, \quad (12)$$

where we introduced

$$\hat{\mathcal{L}}^{(n)} = \nu_{\text{shift}}^{(n)} \hat{\mathcal{L}}_{\text{shift}}^{(n)} + \nu_{\text{spin}}^{(n)} \hat{\mathcal{L}}_{\text{spin}}^{(n)}. \quad (13)$$

For $M_n = M'_n = 0$, one defines the four states $|\rho_z = \pm 1; \sigma_z = \pm 1\rangle$ in $\rho \otimes \sigma$ space. Two of these give rise to the pair of nodes at $\pm\mathbf{k}_n$, while the remaining two lie energetically away from zero. These two pairs of states can be distinguished by their helicity eigenvalue $\zeta = \rho_z \sigma_z = \pm 1$. Hence, to obtain a Hamiltonian describing only the states related to the nodes, we project Eq. (10) onto a given helicity subspace which fulfills:

$$\varepsilon_s^{(n)} + \zeta \varepsilon_t^{(n)} = \Delta_s^{(n)} + \zeta \Delta_t^{(n)} = 0,$$

and end up with the following effective Hamiltonian for the n th pair of nodes

$$\hat{\mathcal{H}}_{\zeta}^{(n)}(\mathbf{q}, \phi = 0) = \lambda_z \mathbf{q} \cdot [\mathbf{v}_{\varepsilon_s, \zeta}^{(n)} \tau_z + \mathbf{v}_{\Delta_s, \zeta}^{(n)} \tau_x] + \mathbf{M}_{\zeta}^{(n)} \cdot \boldsymbol{\lambda}, \quad (14)$$

where we introduced the velocities

$$\mathbf{v}_{\varepsilon_s, \zeta}^{(n)} = \zeta \mathbf{v}_{\varepsilon_s}^{(n)} + \mathbf{v}_{\varepsilon_t}^{(n)} \quad \text{and} \quad \mathbf{v}_{\Delta_s, \zeta}^{(n)} = \zeta \mathbf{v}_{\Delta_s}^{(n)} + \mathbf{v}_{\Delta_t}^{(n)} \quad (15)$$

along with the parameters

$$\mathbf{M}_{\zeta}^{(n)} = (\hat{\varepsilon}_{n,x} M_n + \zeta \hat{\varepsilon}'_{n,y} M'_n, \hat{\varepsilon}_{n,y} M_n - \zeta \hat{\varepsilon}'_{n,x} M'_n, 0), \quad (16)$$

which quantify the influence of the MTC on the given pair of nodes. The unit $\mathbb{1}_{\lambda}$ and Pauli $\boldsymbol{\lambda}$ matrices act in a given helicity subspace. The choice of basis for both $\zeta = \pm 1$ is such, so that the spin Pauli matrix σ_z coincides with λ_z . Note that the terms $\hat{\mathbf{e}}_n \cdot \hat{\mathbf{z}}$ and $\hat{\mathbf{e}}'_n \cdot \hat{\mathbf{z}}$ drop out after the projection. Projecting the operator generating the vortices yields

$$\hat{\mathcal{L}}_{\zeta}^{(n)} = [\zeta \nu_{\text{shift}}^{(n)} + \nu_{\text{spin}}^{(n)}] \lambda_z. \quad (17)$$

Notably, the emergence of MZMs is guaranteed by the structure of Eqs. (14) and (17), which allow mapping our model to the Jackiw-Rossi model [90]. The latter is known to support zero-energy solutions in vortices, and also lies at the core of the Fu-Kane MZM proposal [7,91].

V. LOW-ENERGY MODEL HAMILTONIAN - BDI CLASS TOPOLOGICAL INVARIANT IN 2D

In this paragraph, we prove in a detailed fashion that MZMs become accessible in the model of Eq. (14). The Hamiltonian in Eq. (14) possesses a chiral symmetry effected by the operator $\Pi = \lambda_z \tau_y$. As a result of it, the Hamiltonian resides in class BDI and is classified by the winding number [58] $w_3^{(n)} \in \mathbb{Z}$ defined in (q_x, q_y, ϕ) space. This invariant is calculated using the upper off-diagonal block $\hat{h}_\zeta^{(n)}(\mathbf{q}, \phi)$ of $\hat{\mathcal{H}}_\zeta^{(n)}(\mathbf{q}, \phi)$, in a basis where the latter is block off-diagonal. The winding number is defined as

$$w_3 = \int_0^{2\pi} \frac{d\phi}{2\pi} \int \frac{d\mathbf{q}}{2\pi} \text{Tr} \{ \hat{h}_\zeta^{-1}(\mathbf{q}, \phi) [\partial_{q_x} \hat{h}_\zeta(\mathbf{q}, \phi)] \times \hat{h}_\zeta^{-1}(\mathbf{q}, \phi) [\partial_{q_y} \hat{h}_\zeta(\mathbf{q}, \phi)] \hat{h}_\zeta^{-1}(\mathbf{q}, \phi) [\partial_\phi \hat{h}_\zeta(\mathbf{q}, \phi)] \}, \quad (18)$$

where we momentarily drop the (n) index for simplicity. Using the relation $\hat{h}_\zeta \hat{h}_\zeta^{-1} = \mathbb{1} \Rightarrow \partial_{q_x} \hat{h}_\zeta^{-1} = -\hat{h}_\zeta^{-1} (\partial_{q_x} \hat{h}_\zeta) \hat{h}_\zeta^{-1}$ and the cyclic property of the trace, we find the equivalent expression:

$$w_3 = - \int_0^{2\pi} \frac{d\phi}{2\pi} \int \frac{d\mathbf{q}}{2\pi} \text{Tr} \{ [\partial_{q_x} \hat{h}_\zeta(\mathbf{q}, \phi)] \hat{h}_\zeta^{-1}(\mathbf{q}, \phi) [\partial_{q_y} \hat{h}_\zeta(\mathbf{q}, \phi)] \partial_\phi \hat{h}_\zeta^{-1}(\mathbf{q}, \phi) \}. \quad (19)$$

Since the following relation also holds

$$\hat{h}_\zeta(\mathbf{q}, \phi) = e^{i\phi \hat{\mathcal{L}}/2} \hat{h}_\zeta(\mathbf{q}, \phi = 0) e^{-i\phi \hat{\mathcal{L}}/2}, \quad (20)$$

the winding number obtains the simplified form:

$$w_3 = \int \frac{d\mathbf{q}}{2\pi i} \text{Tr} \left\{ \frac{\hat{\mathcal{L}}}{4} \{ [\partial_{q_x} \hat{h}_\zeta(\mathbf{q}, \phi = 0)] [\partial_{q_y} \hat{h}_\zeta^{-1}(\mathbf{q}, \phi = 0)] - [\partial_{q_x} \hat{h}_\zeta^{-1}(\mathbf{q}, \phi = 0)] [\partial_{q_y} \hat{h}_\zeta(\mathbf{q}, \phi = 0)] - q_x \leftrightarrow q_y \} \right. \\ \left. = \int \frac{d\mathbf{q}}{2\pi} \text{Tr} \left\{ \frac{\hat{\mathcal{L}}}{2} \mathcal{O}_{q_x q_y} i \ln [\hat{h}_\zeta(\mathbf{q}, \phi = 0)] \right\}, \quad (21)$$

where we introduced the shorthand notation:

$$\mathcal{O}_{q_x q_y} = \partial_{q_x} \partial_{q_y} - \partial_{q_y} \partial_{q_x},$$

for the differential operator defining vorticity in \mathbf{q} space.

The above expression is nonzero even in the limit of a vanishing strength for the MTC, in which case, $\hat{h}(\mathbf{q}, \phi = 0) \mapsto \hat{h}_0(\mathbf{q})$. When $[\hat{\mathcal{L}}, \hat{h}_0(\mathbf{q})] = \hat{0}$, we evaluate the trace by introducing the eigenstates of $\hat{\mathcal{L}}$, in which basis, $\hat{h}_0(\mathbf{q})$ is block diagonal. Hence, by further making use of

$$\hat{h}_\zeta^{(n)}(\mathbf{q}, \phi) = e^{i\phi \hat{\mathcal{L}}_\zeta^{(n)}/2} \hat{h}_\zeta^{(n)}(\mathbf{q}, \phi = 0) e^{-i\phi \hat{\mathcal{L}}_\zeta^{(n)}/2} \quad (22)$$

and taking into account that the upper off-diagonal block $\hat{h}_{0;\zeta}^{(n)}(\mathbf{q})$ of $\hat{\mathcal{H}}_{0;\zeta}^{(n)}(\mathbf{q})$ commutes with $\hat{\mathcal{L}}^{(n)}$, we obtain

$$w_{3;\zeta}^{(n)} = \sum_{\lambda=\pm 1} \frac{\zeta v_{\text{shift}}^{(n)} + v_{\text{spin}}^{(n)}}{2} \lambda \int \frac{d\mathbf{q}}{2\pi} \mathcal{O}_{q_x q_y} i \text{tr} \ln [\hat{h}_{0;\zeta}^{(n)}(\mathbf{q})], \quad (23)$$

where we employed the eigenstates $|\lambda\rangle$ of $\hat{\mathcal{L}}_\zeta^{(n)}$, which here coincide with the eigenstates of $\lambda_z = \pm 1$. In addition, we accordingly restricted the trace Tr , to a trace tr over the

remaining degrees of freedom. By now making use of the identity $\text{tr} \ln [\hat{h}_{0;\zeta}^{(n)}(\mathbf{q})] = \ln \det [\hat{h}_{0;\zeta}^{(n)}(\mathbf{q})]$, we write

$$\det [\hat{h}_{0;\zeta}^{(n)}(\mathbf{q})] = |\det [\hat{h}_{0;\zeta}^{(n)}(\mathbf{q})]| e^{-i\varphi_{\zeta,\lambda}^{(n)}(\mathbf{q})}. \quad (24)$$

The above implies that Eq. (23) is nonzero only when the arguments $\varphi_{\zeta,\lambda}^{(n)}(\mathbf{q})$ contain \mathbf{q} -space vortex defects, i.e., *only when the underlying SC contains point nodes*.

The node with helicity ζ and z -axis spin projection $\sigma_z = \pm 1$, carries vorticity $v_{\zeta,\lambda=\pm 1}^{(n)}$, which is defined through the relation

$$\mathcal{O}_{q_x q_y} \varphi_{\zeta,\lambda}^{(n)}(\mathbf{q}) = 2\pi v_{\zeta,\lambda}^{(n)} \delta(\mathbf{q}) \quad (25)$$

and leads to the expression:

$$w_{3;\zeta}^{(n)} = \sum_{\lambda=\pm 1} \frac{\zeta v_{\text{shift}}^{(n)} + v_{\text{spin}}^{(n)}}{2} \lambda v_{\zeta,\lambda}^{(n)}. \quad (26)$$

To evaluate the above, it is required to determine the vorticities of the nodes. For this purpose, we consider the unitary transformation $(\Pi + \tau_z)/\sqrt{2}$ onto the projected Hamiltonians, and obtain the upper off-diagonal blocks:

$$\hat{h}_\zeta^{(n)}(\mathbf{q}, \phi = 0) = [\mathbf{M}_\zeta^{(n)} \times \hat{\mathbf{z}}] \cdot \boldsymbol{\lambda} - \mathbf{q} \cdot [\mathbf{v}_{\Delta,\zeta}^{(n)} \lambda_z + i\mathbf{v}_{\varepsilon,\zeta}^{(n)}]. \quad (27)$$

We use the eigenstates of $\lambda_z \mapsto \lambda = \pm 1$ and diagonalize $\hat{h}_{0;\zeta}^{(n)}(\mathbf{q})$ as $h_{0;\zeta,\lambda}^{(n)}(\mathbf{q}) = -\mathbf{q} \cdot [\lambda \mathbf{v}_{\Delta,\zeta}^{(n)} + i\mathbf{v}_{\varepsilon,\zeta}^{(n)}]$. Therefore, as long as $\mathbf{v}_{\varepsilon,\zeta}^{(n)} \times \mathbf{v}_{\Delta,\zeta}^{(n)} \neq \mathbf{0}$, the vorticities of the nodes at $\mathbf{q} = \mathbf{0}$ are opposite and of a single unit, hence, they satisfy $v_{\zeta,-\lambda}^{(n)} = -v_{\zeta,\lambda}^{(n)}$ and $|v_{\zeta,\lambda}^{(n)}| = 1$.

Under the above conditions, we obtain *our main result*:

$$w_{3;\zeta}^{(n)} = \text{sgn}[v_{\zeta,\lambda=+1}^{(n)}] [\zeta v_{\text{shift}}^{(n)} + v_{\text{spin}}^{(n)}], \quad (28)$$

which implies that both spin and shift vortex defects can independently induce a \mathbb{Z} number of MZMs. Notably, the number of MZMs arising due to the simultaneous emergence of shift and spin vortices at the same position in coordinate space, are obtained by adding (for $\zeta = 1$) or subtracting (for $\zeta = -1$) the number of MZMs that would independently arise for each different type of defect.

VI. NUMERICAL CALCULATIONS IN 2D

In this section, we numerically verify our above predictions for a variety of models in symmetry classes BDI, D, and DIII. Our starting point for all these investigations is the lattice model defined by the following functions:

$$\varepsilon_s(\mathbf{k}) = -2t(\cos k_x + \cos k_y) - \mu, \quad \varepsilon_t(\mathbf{k}) = \alpha \sin k_y, \\ \Delta_s(\mathbf{k}) = \Delta \quad \text{and} \quad \Delta_t(\mathbf{k}) = d_z \sin k_y. \quad (29)$$

In the absence of magnetism and for a suitable window of parameters, this model supports a nodal energy spectrum of the form depicted in Fig. 1(a). For our upcoming numerical simulations we consider a 40×40 square lattice with the lattice constant set to unity. Moreover, all the energy scales are expressed in units of t , which from now on is set to unity.

A. Symmetry class BDI models

We begin with the study of MZMs in a BDI class model in 2D. We consider that the two pairs of nodes emerging in

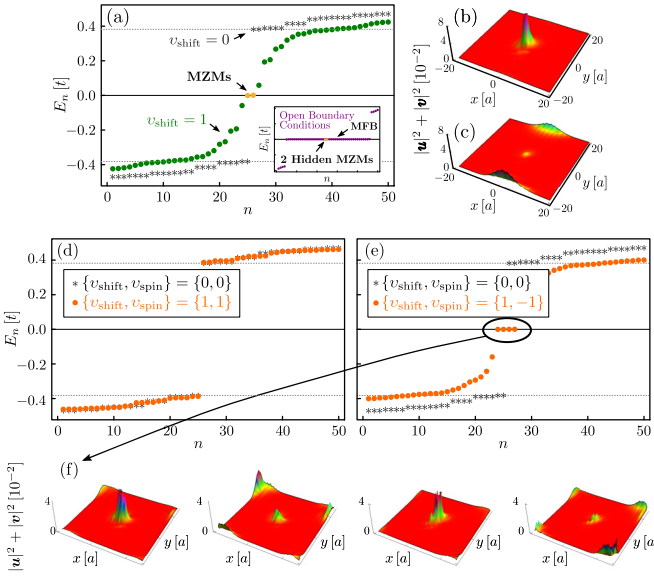


FIG. 2. (a) 50 lowest eigenvalues in the absence (black asterisks) and presence (green dots) of a single shift vortex in the MTC with $v_{\text{shift}} = 1$. When considering open boundary conditions, see inset in (a), we find a single MZM pair along with an edge Majorana flat band (MFB). To uncover the MZMs which are energetically buried inside the MFB, we employ instead periodic boundary conditions. [(d) and (e)] The 50 lowest eigenvalues in the absence (black asterisks) and presence (orange dots) of a composite spin-shift vortex defect with $\{v_{\text{shift}}, v_{\text{spin}}\} = \{1, \pm 1\}$, respectively. In accordance to Eq. (28) only the latter leads to MZMs. (b), (c), and (f) depict the spatial distribution of the MZM eigenvectors. For extracting the above numerical results, we considered the following values for the parameters of the model in Eq. (29): $\Delta = 1/\sqrt{2}$, $\mu = -5\Delta$, $d_z = \alpha = 1$, and $\{M_{1,2}, M'_{1,2}\} = \{0.5, 0.1\}$.

the energy spectrum of the model in Eq. (29) get gapped out by a MTC which consists of two helices $M_{1,2}(\mathbf{r})$, with wave vectors $\mathcal{Q}_{1,2}$. In Fig. 2, we present results for helices with $\{\hat{e}_{1,2}, \hat{e}'_{1,2}\} = \{\hat{x}, \hat{y}\}$, when only one of these two magnetic helices harbors a shift vortex defect of a single unit of vorticity.

In accordance with the analytical predictions of Eq. (28), our numerical results presented in Figs. 2(a)–2(c) confirm the emergence of a single MZM pair. One of the MZMs is trapped at the shift defect’s core, while the other appears at the system’s edge. Moreover, the MZM pair comes along with an edge Majorana flat band (MFB). The latter results from the nodal character of the SC and would anyhow be present at the edge of the system independently of the presence of the vortex.

We remark that the vortex MZM and the MFB do not couple since their wave functions have negligible spatial overlap. Panels (b) and (c) of Fig. 2 depict the spatial distribution of the eigenvectors for the two MZMs found in (a). We denote the electron (hole) column component of the eigenvectors with \mathbf{u} (\mathbf{v}). One observes that finite-size effects introduced a weak inter-MZM coupling, which in turn leads to a small but nonzero MZM weight at the defect in (c).

Furthermore, in Figs. 2(d)–2(f), we numerically confirm the predictions of Eq. (28) in the case of simultaneous spin and

shift vortex defects appearing at the same location in real coordinate space \mathbf{r} . According to Eq. (28), the final outcome for the winding number $w_{3;\zeta}$ for the pair of nodes experiencing the combined vortex defects is given by adding or subtracting the independent contributions of each vortex to the winding number. Whether these add up or subtract solely depends on which helicity eigenvalue $\zeta = +1$ or for $\zeta = -1$ characterizes the nodes of interest. Specifically, for the model of Eq. (29) and the parameter values employed, we conclude that $\zeta = -1$. This is directly inferable from the energy spectra shown in Figs. 2(d) and 2(e) for $\{v_{\text{shift}}, v_{\text{spin}}\} = \{1, \pm 1\}$, where we find that only the latter composite vortex configuration leads to MZMs. In fact, one obtains a total of four MZMs, with two of these being located at the center of the defect, and two more near the edge. This becomes further transparent from Fig. 2(f) where we depict the spatial weights of the MZM eigenvectors. We observe once again that the four MZMs appearing in Fig. 2(e) are weakly coupled due to finite-size effects.

The two MZMs comprising the MZM pair appearing at the core of the composite spin-shift vortex with $\{v_{\text{shift}}, v_{\text{spin}}\} = \{1, -1\}$ do not couple to each other by virtue of the chiral symmetry which dictates the system. Notably, multiple uncoupled MZMs trapped at the core of the vortex are also expected to appear for a single shift/spin vortex when this carries a higher value of vorticity. To further verify this prediction, we study various cases numerically, by implementing the same lattice Hamiltonian defined by Eq. (29). In Figs. 3(a) and 3(c), we confirm that $v_{\text{shift}} = 2$ results into two pairs of MZMs, with two at the center of the defect, and their two partners on the edge. Additionally we confirm that spin defects also lead to MZMs. See Fig. 3(d) with three pairs of MZMs now appearing at the vortex core for $v_{\text{spin}} = 3$.

B. Class D models in 2D

The result of Eq. (28) obtained earlier is valid *only* as long as also the full Hamiltonian resides in class BDI. In fact, it is straightforward to verify that the full Hamiltonian possesses a chiral symmetry effected by $\tau_y \sigma_z$, only when \mathbf{e}_n and \mathbf{e}'_n lie in the same spin plane for all n . When at least one of $\varepsilon_t(\mathbf{k})$ or $\Delta_t(\mathbf{k})$ is present, this is identified with the xy spin plane. As long as the above condition is met, Eq. (28) remains valid.

For a full Hamiltonian belonging to class D instead, solely the parity of the winding number $(-1)^{w_{3;\zeta}^{(n)}} \in \mathbb{Z}_2$ is well defined, and allows for only up to a single MZM to be trapped at the core of a vortex defect.

The above conclusions further imply that particular caution needs to be paid on the possible node degeneracies which can trivialize the \mathbb{Z}_2 invariant. This takes place, for instance, when only $\varepsilon_s(\mathbf{k})$ and $\Delta_s(\mathbf{k})$ enter $\hat{H}_0(\mathbf{k})$. In this case, both helicities contribute, i.e., $w_3^{(n)} = \sum_{\zeta=\pm 1} w_{3;\zeta}^{(n)}$. This case is trivial in class D, since we find $|w_3^{(n)}| = 2|v_{\text{spin}}^{(n)}|$, while in class BDI it predicts spin-degenerate MZM pairs only for spin vortices, as a consequence of the spin-singlet character of the pairing. Analogous results with $|w_3^{(n)}| = 2|v_{\text{shift}}^{(n)}|$ are obtained when only $\varepsilon_s(\mathbf{k})$ and $\Delta_t(\mathbf{k})$ are considered.

We now proceed with scenarios where a symmetry class transition $\text{BDI} \mapsto \text{D}$ takes place by explicitly breaking the

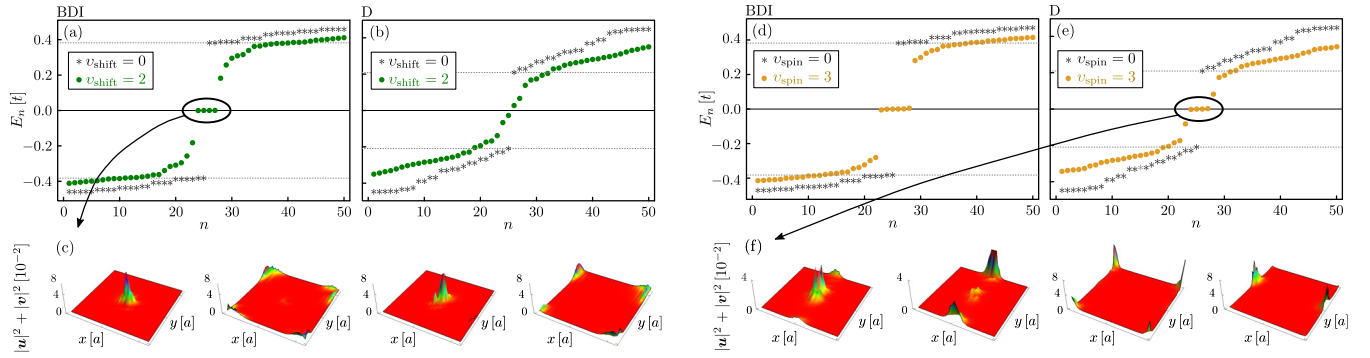


FIG. 3. [(a) and (b)] The 50 lowest eigenvalues in the absence (black asterisks) and presence (green dots) of a shift vortex defect with two units of vorticity $v_{\text{shift}} = 2$ for a class BDI and D model, respectively. In (b), we observe that a class D model does not support MZMs for $v_{\text{shift}} = 2$, in agreement with the invariant defined as the parity of $w_{3;\zeta}^{(n)}$. As indicated by the arrow, we show in (c) the weight of the MZM wavefunctions, where we clearly see two states located at the defect and their charge-conjugate counterparts at the edge of the system. [(d)–(f)] Same as in (a)–(c) but in the case of a single spin defect with three units of vorticity $v_{\text{spin}} = 3$. For the class D model in (e), we expect a single MZM pair, in agreement with the parity of $w_{3;\zeta}^{(n)}$, yet we observe four zero energy states. The additional two states, see the two last panels in (f), are an artifact of the phase jump at the edges of the system, and are therefore not located at the defect. For our numerics, we employed the same parameter values as in Fig. 2. For the class D cases, we considered an additional magnetic field of strength $B_z = 0.4$.

chiral symmetry of Eq. (3), which is effected by $\tau_y \sigma_z$. In the simplest case, this can be achieved by either applying a magnetic field in the z direction, or, by considering spin-orientation vectors \mathbf{e}_n and \mathbf{e}'_n which lie in different spin planes. By virtue of the symmetry class reduction, it is only the parity $(-1)^{w_{3;\zeta}^{(n)}}$ which can protect MZMs.

This is confirmed in Fig. 3(b) where we display the energy spectrum for $v_{\text{shift}} = 2$ in the presence of a magnetic field in the z direction, here denoted B_z , which enters in the Hamiltonian of Eq. (3) through the term $B_z \sigma_z$. For this case $(-1)^{w_{3;\zeta}^{(n)}} = 1$, ultimately resulting into the hybridization of the MZMs, thus lifting them away from zero energy. In stark contrast, if we have an odd number of MZMs, i.e., $(-1)^{w_{3;\zeta}^{(n)}} = -1$, a single pair of MZM persists in the presence of a magnetic field in z direction, as seen in Figs. 3(e) and 3(f). We wish to clarify that despite the fact that in Fig. 3(e) we find four in-gap states, only a single pair corresponds to topologically protected MZMs, with only one of these MZMs having its wave-function weight localized at the defect, as one confirms from Fig. 3(f).

C. Class DIII Models in 2D

Despite the fact that MTCs break the standard time reversal (\mathcal{T}) symmetry, Majorana Kramers pairs are still accessible when a generalized TR symmetry Θ with $\Theta^2 = -\mathbb{1}$ appears instead [68]. In this event, the Hamiltonian is of the DIII type and is classified by a \mathbb{Z}_2 topological invariant which now predicts the emergence of a single Majorana Kramers pair in a shift/spin vortex.

Such a symmetry emerges in the previously examined models when we consider, for instance, two bands labeled by a and b . After introducing the κ Pauli matrices in band space, the MTC terms contributing to the BdG Hamiltonian get promoted to matrices in band space, allowing for intra- and interband magnetic scattering terms proportional to $\mathbb{1}_\kappa$, κ_z and κ_x , respectively. In the remainder, we consider solely intraband magnetic scattering, with the magnetic texture term

being proportional to κ_z . Hence, the two bands feel opposite contributions from the MTCs.

After considering that the two bands are dictated by identical nonmagnetic terms given by Eq. (4), we end up with the following Hamiltonian for a two-band system:

$$\hat{\mathcal{H}}'(\hat{\mathbf{p}}, \mathbf{r}) = \hat{\mathcal{H}}_0(\hat{\mathbf{p}}) + \sum_n \{ 2M_n \cos[\mathbf{Q}_n \cdot \mathbf{r} + \eta_n(\mathbf{r})] \hat{\mathbf{e}}_n - 2M'_n \sin[\mathbf{Q}_n \cdot \mathbf{r} + \eta_n(\mathbf{r})] \hat{\mathbf{e}}'_n \} \cdot \kappa_z \sigma e^{-i\omega_n(\mathbf{r})\sigma_z}. \quad (30)$$

Since the above bands are completely decoupled, they yield pairs of Majorana solutions in the defect's core. Specifically, we find that the pair of MZMs is protected by the time-reversal symmetry $\Theta = \kappa_x \mathcal{T}$. Notably, the above Hamiltonian possesses an additional U(1) symmetry with generator κ_z , which enlists the present system in class BDI \oplus BDI, instead of DIII. Hence, in order to obtain true Majorana Kramers pairs protected by Θ it is required to include band mixing terms which are simultaneously invariant under the action of Θ .

In order to numerically study class DIII models in 2D, we consider the lattice extension of the two band Hamiltonian in Eq. (30), in the additional presence of the weak band mixing term $\delta\tau_z \kappa_x$ which preserves Θ . We focus on the two-band extension of the 2D BDI model in Eq. (29) where, here, we set $\varepsilon_t^a(\mathbf{k}) = \varepsilon_t^b(\mathbf{k}) = \alpha \sin k_y$, $\Delta_s^a(\mathbf{k}) = \Delta_s^b(\mathbf{k}) = 0$ and $\Delta_t^a(\mathbf{k}) = \Delta_t^b(\mathbf{k}) = d_z \sin k_x$. Our numerics confirm the emergence of a MZM Kramers pair when considering a single shift/spin vortex defect, as seen in Fig. 4(a) where we observe four MZMs. The spatially resolved MZM wave-function weights in Fig. 4(c) show that one MZM Kramers pair is localized at the defect and another at the outer edge of the system.

Similarly to the BDI models in 2D, we can also here reduce the symmetry of the system by adding a homogeneous external magnetic field. In Fig. 4(b), we indeed see that the MZM Kramers pair is lifted away from zero energy by adding a magnetic field in the z direction, which forces the TR-invariant system to undergo a symmetry-class transition to class D. The latter supports a \mathbb{Z}_2 invariant and cannot sustain the MZM Kramers pair.

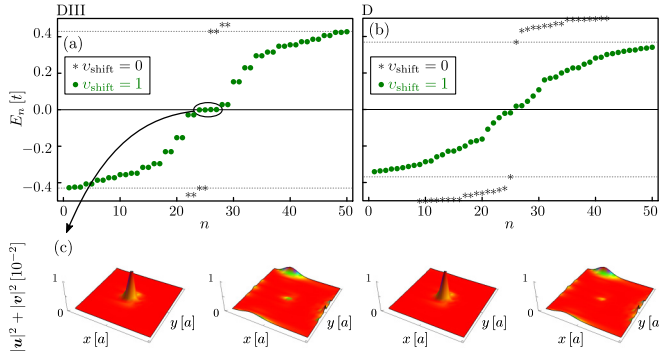


FIG. 4. Numerical investigation of a 2D class DIII model and its transition to a class D model. [(a) and (b)] The 50 lowest eigenvalues in the absence (black asterisks) and presence (green dots) of a shift vortex with $v_{\text{shift}} = 1$, for the two-band extension of the BDI model in 2D, ultimately resulting into a class DIII. (c) displays the resulting four zero energy states from the MZM Kramers pair, and (b) shows how these get lifted in the presence of a magnetic field of a strength $B_z = 0.4$, entering through the term $B_z \sigma_z$. For the DIII model numerics we used: $\mu = -2\sqrt{2}$, $\alpha = 2 + \mu$, $d_z = 1$, $\{M_1, M'_1\} = \{1, 0.2\}$, $\{M_2, M'_2\} = \{0.5, 0.5\}$, and the band mixing term $\delta_0 = 0.2\sqrt{2}$. Note that finite-size effects, and inter MZM coupling result into weights at the defect in the second and fourth panels of (c).

To this end, we clarify that while Θ appears to be a fine-tuned symmetry which crucially depends on the here-assumed structure of the MTC, it may actually constitute a robust symmetry in realistic materials. This is, for instance, the case when the MTC develops spontaneously due to interactions. In such a scenario, a MTC changing sign on the two bands which is self-generated by the electrons of the SC is expected to be thermodynamically stable, since its emergence leads to a global minimum of the free energy the system.

VII. LOW-ENERGY MODEL HAMILTONIAN - D CLASS TOPOLOGICAL INVARIANT IN 3D

Having examined 2D systems in detail, we now proceed with exploring topological scenarios in 3D. Based on our topological analysis in Sec. III, 3D allows for two possibilities. Chiral/helical Majorana edge modes dispersing along a vortex line arising from a class D/DIII Hamiltonian. The construction of a class DIII Hamiltonian is possible by putting together two class D Hamiltonians following the prescription of the previous section. Since DIII class systems can be understood using an even number of class D copies, in the remainder we focus on the topological aspects of a single class D Hamiltonian.

The emergence of a chiral vortex Majorana mode is now predicted by a second Chern number C_2 which is defined in 4D $(q_x, q_y, \phi, q_z) \equiv (p_1, p_2, p_3, p_4)$ space and it is given by the following expression [58]:

$$C_2 = - \int \frac{d^4 p}{32\pi^2} \epsilon_{nm\ell s} \text{Tr}[\hat{F}_{nm} \hat{F}_{\ell s}], \quad (31)$$

with $\epsilon_{nm\ell s}$ denoting the fully antisymmetric tensor, where $n, m, \ell, s = 1, 2, 3, 4$. We also note that repeated index summation was employed. The above formula is given in terms of

the non-Abelian field strength tensor:

$$\hat{F}_{nm} = \partial_{p_n} \hat{A}_m - \partial_{p_m} \hat{A}_n - i[\hat{A}_n, \hat{A}_m], \quad (32)$$

which is defined in terms of the Berry vector potential:

$$A_n^{\alpha\beta}(\mathbf{p}) = i \langle \Phi_\alpha(\mathbf{p}) | \partial_{p_n} | \Phi_\beta(\mathbf{p}) \rangle, \quad (33)$$

which is a matrix in the occupied eigenstates $|\Phi_\alpha(\mathbf{p})\rangle$ subspace, which are enumerated by the index α .

The second Chern number can be equivalently expressed as a surface integral over the Chern-Simons 3 form. Here, we choose a surface $\mathcal{S} = \mathbb{S}^2 \times \mathbb{T}^1$ which contains a \mathbb{S}^2 sphere in \mathbf{q} space. We thus find

$$C_2 = - \oint_{\mathcal{S}} \frac{d^3 p}{8\pi^2} \epsilon_{nm\ell} \text{Tr} \left(\hat{A}_n \partial_{p_m} \hat{A}_\ell - i \frac{2}{3} \hat{A}_n \hat{A}_m \hat{A}_\ell \right), \quad (34)$$

with $n, m, \ell = 1, 2, 3$. When the following holds:

$$\hat{\mathcal{H}}(\mathbf{q}, \phi) = e^{i\phi \hat{\mathcal{L}}/2} \hat{\mathcal{H}}(\mathbf{q}, \phi = 0) e^{-i\phi \hat{\mathcal{L}}/2}, \quad (35)$$

we find the relation: $|\Phi(\mathbf{q}, \phi)\rangle = e^{i\phi \hat{\mathcal{L}}/2} |\Phi(\mathbf{q}, \phi = 0)\rangle$, which implies $\hat{A}_q(\mathbf{q}, \phi) = \hat{A}_q(\mathbf{q}, \phi = 0)$ and

$$A_\phi^{\alpha\beta}(\mathbf{q}, \phi) = -\frac{1}{2} \langle \Phi_\alpha(\mathbf{q}, \phi = 0) | \hat{\mathcal{L}} | \Phi_\beta(\mathbf{q}, \phi = 0) \rangle. \quad (36)$$

The above lead to the simplified expression:

$$C_2 = \iint_{\mathbb{S}^2} \frac{d\mathbf{q}}{2\pi} \cdot \text{Tr} \left[\frac{\hat{\mathcal{L}}}{2} \hat{\Omega}(\mathbf{q}, \phi = 0) \right], \quad (37)$$

where we introduced the matrix Berry curvature $\hat{\Omega}(\mathbf{q}, \phi = 0)$. The second Chern number is here generally nonzero also for a vanishing MTC strength. Under the assumption $[\hat{\mathcal{L}}, \hat{\mathcal{H}}_0(\mathbf{q})] = \hat{0}$, we evaluate the trace by introducing the eigenstates of $\hat{\mathcal{L}}$, i.e., $\hat{\mathcal{L}}|\lambda\rangle = \nu_{\text{defect}} \lambda |\lambda\rangle$, in which basis, $\hat{\mathcal{H}}_0(\mathbf{q})$ and the respective Berry curvature matrix $\hat{\Omega}_0(\mathbf{q})$ of the nonmagnetic system are block diagonal. Thus we conclude with the expression

$$C_2 = \nu_{\text{defect}} \sum_{\lambda} \frac{\lambda}{2} \iint_{\mathbb{S}^2} \frac{d\mathbf{q}}{2\pi} \cdot \text{tr}[\hat{\Omega}_{0;\lambda}(\mathbf{q})], \quad (38)$$

with the trace acting in a given λ block. Under the assumption that the SCs under examination possess a zero first Chern number, the second Chern number above becomes nonzero only in the presence of monopoles in the Berry curvature of the SC. These monopoles correspond to \mathbf{q} -space nodes in 3D space, which carry a topological charge defined through $\text{tr}[\hat{\Omega}_{0;\lambda}(\mathbf{q})] = Q_{\lambda} \mathbf{q} / (2|\mathbf{q}|^3)$. For a 2×2 λ block, these monopoles define Weyl points, which carry a topological charge given by

$$\Omega_{0;\lambda}(\mathbf{q}) = Q_{\lambda} \frac{\mathbf{q}}{2|\mathbf{q}|^3}. \quad (39)$$

From the above relation, we obtain the conclusive expression for the invariant, which takes the following form:

$$C_{2;\zeta}^{(n)} = \sum_{\lambda=\pm 1} \frac{\zeta \nu_{\text{shift}}^{(n)} + \nu_{\text{spin}}^{(n)}}{2} \lambda Q_{\zeta;\lambda}^{(n)}, \quad (40)$$

with $Q_{\zeta;\lambda}^{(n)}$ defining the monopole charge for the nodes of the n th path with helicity ζ and z -axis spin projection $\lambda = \pm 1$.

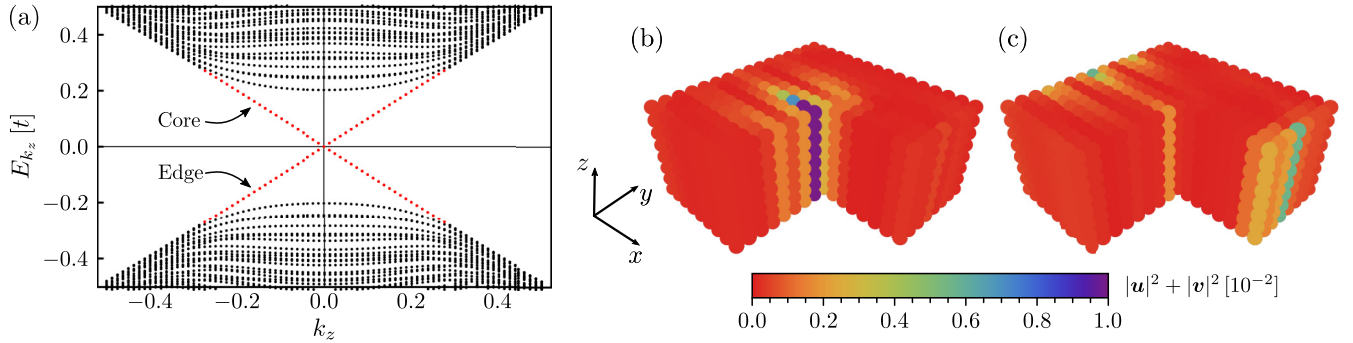


FIG. 5. Chiral Majorana modes in a class D model in 3D. (a) Edge spectrum for the 3D model with a single shift vortex defect $v_{\text{shift}} = 1$. The spectrum is obtained with periodic (open) boundary conditions in the z (x and y) direction, and clearly displays chiral Majorana modes. The spatially-resolved weight of the two chiral branches are displayed in (b) and (c), and reveals a single Majorana mode at the vortex defect's core, and its counterpart located at the edge of the system. Note that the nonzero wave-function weight at the defect in (c), is a consequence of inter-Majorana mode coupling and finite-size effects. The figures were obtained with the parameters: $\Delta = 1$, $\mu = -2\sqrt{2}$, $\alpha = 2(\sqrt{2} - 1)$, $\Lambda = 8$ and $\{M_{1,2}, M'_{1,2}\} = \{0.5, 0.1\}$, all in units of t .

VIII. NUMERICAL CALCULATIONS FOR A D CLASS 3D MODEL

The topological invariant C_2 obtained in the previous paragraph predicts the number of chiral Majorana modes emerging in the core of a vortex line. We first pursue gaining insight regarding the emergence of such dispersive chiral vortex Majorana modes using the following simple continuum model:

$$\hat{\mathcal{H}}_0(\mathbf{k}) = -k_y^2 \tau_z + \alpha(k_y \tau_z + k_x \tau_x - k_z \tau_y) \sigma_z, \quad (41)$$

which constitutes an anisotropic p -wave SC variant of the model in Eq. (29). The combination of spatial anisotropy and SOC yields two helical branches and two pair of nodes at $k_y = 0$ and $k_y = \pm\alpha$. Here, the inner helical branch at $k_y = 0$ can be gapped out by a Zeeman field which is oriented orthogonally to the SOC vector [10,11]. The two nodes of the outer helical branch can get gapped out by a magnetic stripe $\mathbf{M}(\mathbf{r}) = M \cos(2\alpha y)\hat{x}$. In analogy to Eq. (28), here we find that a number of

$$|C_2| = |v_{\text{shift}} + v_{\text{spin}}| \quad (42)$$

chiral Majorana modes emerge in a vortex line extending along the z axis.

We now provide a numerical investigation of the above class D model in 3D, after considering a proper lattice extension. For this purpose, we consider that the bare Hamiltonian of Eq. (4) is given by

$$\hat{\mathcal{H}}_0^{3D}(\mathbf{k}) = \tau_z[\varepsilon_s(\mathbf{k}) + \varepsilon_t(\mathbf{k})\sigma_z] + [\Delta_p(\mathbf{k})\tau_x + \Delta'_p(\mathbf{k})\tau_y]\sigma_z \quad (43)$$

and consists of the anisotropic 3D dispersion

$$\varepsilon_s(\mathbf{k}) = -2t(\cos k_x + \cos k_y) - \Lambda(1 - \cos k_z)/2 - \mu$$

in the additional presence of the anisotropic SOC term $\varepsilon_t(\mathbf{k}) = \alpha \sin k_y$, and the chiral p -wave pairing which is defined in terms of the components:

$$\Delta_p(\mathbf{k}) = \Delta \sin k_x \quad \text{and} \quad \Delta'_p(\mathbf{k}) = -\Delta \sin k_z. \quad (44)$$

We consider the limit $\Lambda \gg t$, in which, the pairs of nodes in the nonmagnetic phase are located only in the $k_z = 0$ plane. After including the magnetic terms of the Hamiltonian and

considering a vortex line which extends uniformly along the z axis, we observe that k_z is a good quantum number since $\tan \phi = y/x$. In fact, for small k_z , we can linearize the above Hamiltonian and see that for $k_z = 0$ it possesses a chiral symmetry with $\Pi = \tau_y \sigma_z$ similar to the model of Eq. (29). The preservation of Π gives rise to a pair of zero energy states.

Away from $k_z = 0$ the chiral symmetry is broken, lifting the states away from zero energy, ultimately resulting into dispersive chiral Majorana modes, as seen Fig. 5(a). Here, a single mode is dispersing along the vortex core while the other one resides on the outer edge of the system, see Figs. 5(b) and 5(c), respectively.

IX. EXPERIMENTAL IMPLEMENTATION

We now proceed with the discussion of potential candidate systems and mechanisms that may allow observing our theoretical predictions in realistic systems. As mentioned above, nodal superconducting materials are abundant in nature [63], e.g., unconventional spin-singlet ($-$ triplet) d -wave (p -wave) SCs [92], noncentrosymmetric [93–96] SCs, and certain Fe-based SCs which can also exhibit nodal pairing [97,98]. Below, we discuss three distinct pathways involving MTCs, which lead to a fully gapped bulk energy spectrum and open perspectives for vortex MZMs.

A. MTCs engineered by nanomagnets

The first possibility is to actually impose the desired MTC externally with the help of tunable magnets. Such a direction has recently picked up substantial theoretical [64,66,78,81,82,84,85] and experimental [36,99] attention in the field of engineered topological superconductivity. Furthermore, in a different context, recent experiments [100] have found evidence for colossal magnetic anisotropy for CoFe_2C magnets with a characteristic dimension of the order of few nanometers. Since the wave vectors controlling the spatial periodicity of the MTC are required to roughly match those connecting pairs of nodes, it may be currently challenging for these state-of-the-art nanomagnetic technologies to be applicable in most of the above listed SCs. This is because most

of these are metals and thus the arising nodes are expected to be connected by wave vectors with a length which relates to the Fermi wave number. Hence, we conclude that the present route for engineering vortex MZMs, by means of imposing MTCs induced by magnets, appears more relevant for very low-density and bad-metal SCs, with Fermi wave numbers in the few nanometer regime.

B. Spontaneously induced MTCs

Another possibility is the interaction-driven MTCs, which can become stabilized in the presence of attractive interactions in the magnetic channel, in order to minimize the free energy of the system. In analogy to 1D spin-density waves [101], which are promoted by the perfect nesting of the two points comprising the Fermi surface, here we expect a MTC to spontaneously appear and gap out the nodes. This is under the condition that other competing instabilities are subdominant to the MTC. The tendency of the system towards the spontaneous development of a magnetic helix crystal which gaps out a single pair of nodes can be here inferred by evaluating the respective spin susceptibility. In fact, the latter can be calculated using the low-energy model of Eq. (14).

For this purpose, we restrict to the n th pair of nodes and consider a magnetic helix crystal with projected components $\mathbf{M}_\xi^{(n)} = (M_{\xi,x}^{(n)}, M_{\xi,y}^{(n)}, 0)$. Moreover, we assume that the magnetic helix crystal is governed by a periodicity given by a wave vector which is equal to the wave vector $2\mathbf{k}_n$ connecting the nodes of the pair of interest. We note that, when the wave vector of the magnetic helix matches the one connecting the nodes, a gap opens on these with an infinitesimally weak strength of $|\mathbf{M}_\xi^{(n)}|$. Nonetheless, a full gap is accessible also for detuned wave vectors, but in that event, a threshold strength of $|\mathbf{M}_\xi^{(n)}|$ has to be reached. In the following, we restrict to the ideal scenario of perfectly matched wave vectors, since this is the configuration that yields the highest susceptibility and thus minimizes the free energy of the system.

In the upcoming analysis, we suppress the (n) index from the various variables to simplify the notation. Since in the absence of magnetism the Hamiltonian in Eq. (14) is dictated by an emergent U(1) symmetry generated by λ_z , we can evaluate the desired susceptibility by considering that only one of the components of the magnetic helix texture, either $M_{\xi,x}$ or $M_{\xi,y}$, is nonzero. Under the above conditions, straightforward calculations in the zero temperature limit yield the susceptibility expression:

$$\chi = \int \frac{d\mathbf{q}}{(2\pi)^2} \frac{1}{\sqrt{[\mathbf{q} \cdot \mathbf{v}_{\varepsilon,\zeta}]^2 + [\mathbf{q} \cdot \mathbf{v}_{\Delta,\zeta}]^2}}. \quad (45)$$

By transferring to polar coordinates $\mathbf{q} = q(\cos \gamma, \sin \gamma)$, and after introducing a cutoff wave number q_c , we end up with the expression

$$\chi = \int_0^{2\pi} \frac{d\gamma}{2\pi} \frac{v_c}{\sqrt{1 + \cos \gamma_0 \cos(2\gamma) + \delta \sin \gamma_0 \sin(2\gamma)}}, \quad (46)$$

where we introduced the density of states $v_c = q_c/(2\pi\bar{v})$ which depends on the cutoff q_c and the average velocity defined as $\bar{v} = \sqrt{(|\mathbf{v}_{\varepsilon,\zeta}|^2 + |\mathbf{v}_{\Delta,\zeta}|^2)}/2$. The final outcome for

χ is decided by the precise values of the parameter $\delta = (|\mathbf{v}_{\varepsilon,\zeta}|^2 - |\mathbf{v}_{\Delta,\zeta}|^2)/(|\mathbf{v}_{\varepsilon,\zeta}|^2 + |\mathbf{v}_{\Delta,\zeta}|^2)$ which encodes the velocity mismatch, and the relative angle $\gamma_0 = \gamma_\varepsilon - \gamma_\Delta$, which is defined in terms of the orientation angles $\gamma_{\varepsilon,\Delta}$ given by $\mathbf{v}_{\varepsilon,\zeta} = |\mathbf{v}_{\varepsilon,\zeta}|(\cos \gamma_\varepsilon, \sin \gamma_\varepsilon)$ and $\mathbf{v}_{\Delta,\zeta} = |\mathbf{v}_{\Delta,\zeta}|(\cos \gamma_\Delta, \sin \gamma_\Delta)$. We note that the final form of Eq. (46) was obtained after the redefinition $\gamma \mapsto \gamma + (\gamma_\varepsilon + \gamma_\Delta)/2$, which does not influence the result.

From Eq. (46), we infer that in contrast to 1D spin-density waves, here, the 2D dimensionality does not generally allow for a logarithmically divergent susceptibility. In fact, for velocity vectors oriented at right angles ($\gamma_0 = \pi/2$) which additionally feature equal lengths ($\delta = 0$), the susceptibility reaches its minimum value $\chi_0 = v_c$. Away from this highly symmetric configuration, the ratio χ/χ_0 increases monotonically. Notably, the susceptibility becomes maximized as the system tends to the extreme anisotropic cases with $\gamma_0/\pi \rightarrow \mathbb{Z}$ for arbitrary δ , or, $|\delta| \rightarrow 1$ for arbitrary γ_0 . Thus the appearance of a MTC generally requires a threshold strength for the interaction which drives magnetism. Noteworthy, this critical strength depends strongly on the cutoff q_c , since χ scales linearly with q_c . Finally, this threshold interaction strength becomes reduced by enhancing the anisotropy of the energy dispersion in the vicinity of the nodes.

Out of the various candidates mentioned earlier, Fe-SCs can support nodal phases, exhibit single- and double- \mathcal{Q} magnetic stripe order [102–112], and can harbor the microscopic coexistence of magnetism and superconductivity [102,113–118]. Moreover, recent theoretical studies [119] predict single- and double- \mathcal{Q} MTCs in doped 122 and 1111 compounds. While the theoretical investigation and experimental support regarding the microscopic coexistence of nodal Fe-SCs and MTCs is still lacking, these systems appear as potential candidates to observe the phenomenology discussed in this section.

C. MTCs induced by localized magnetic moments

The last possible physical realization of our theory relies on nodal SCs coupled with lattices of localized magnetic moments. Here, the MTC required for gapping out the nodes of the SC is considered to result from the magnetization of the localized moments. This third mechanism that we propose for engineering MZMs bears similarities to the ones proposed [67,69–75,79,80,120–123] for MZM platforms relying on magnetic chains [42–49]. However, here, the dimension of the lattice of the magnetic impurities needs to coincide with the dimension of the lattice defined by the nodal SC, akin to the picture that holds for Kondo lattice systems [124], which are typical scenarios for rare-earth [65] and heavy-fermion SCs [63,92]. Moreover, we remind the reader that within our proposal MZMs are trapped by vortices of the MTCs instead of termination edges or domain walls. Interestingly, employing MTC vortices for trapping MZMs appears particularly attractive in the case of hybrid systems involving magnetic adatoms, since MTC vortices can be in principle tailored using spin-polarized scanning tunneling microscopy [45,47–49]. The latter technique, further allows for the spin-sensitive detection of the vortex MZMs [123].

In a similar fashion to proposals for self-organized MZM platforms using magnetic adatom chains [70–72], also here, we expect for the magnetization of the magnetic moment lattice to exhibit a spatial profile which reflects the structure of the nodes of the host SC. This profile is determined by the spin susceptibility $\chi_{nm}^{\alpha\beta}$ which couples the magnetic moments through the Ruderman-Kittel-Kasuya-Yosida (RKKY) type of energy term:

$$E_{\text{RKKY}} = -\frac{J^2}{2} \sum_{n,m} \sum_{\alpha,\beta} S_n^\alpha \chi_{\alpha\beta}(\mathbf{R}_n - \mathbf{R}_m) S_m^\beta, \quad (47)$$

where the indices n, m label the impurity lattices sites $\mathbf{R}_{n,m}$, while $\alpha, \beta = x, y, z$ label the spin components of the moments. J denotes the strength of the magnetic exchange coupling between the moment and the electron spin. For a homogeneous nodal SC of a spatial dimension d , the spin susceptibility depends only on the difference $\mathbf{R} = \mathbf{R}_n - \mathbf{R}_m$ of the position vectors of the coupled magnetic moments and is defined by the expression

$$\chi_{\alpha\beta}(\mathbf{R}) = -\frac{1}{2} \int_{-\infty}^{+\infty} \frac{d\epsilon}{2\pi} \text{Tr}[\sigma_\alpha \hat{G}_0(\epsilon, \mathbf{R}) \sigma_\beta \hat{G}_0(\epsilon, -\mathbf{R})], \quad (48)$$

where we introduced the bare matrix Green function

$$\hat{G}_0(\epsilon, \mathbf{R}) = \int \frac{d\mathbf{k}}{(2\pi)^d} e^{i\mathbf{k}\cdot\mathbf{R}} \hat{G}_0(\epsilon, \mathbf{k}), \quad (49)$$

with its momentum space counterpart being defined through: $\hat{G}_0^{-1}(\epsilon, \mathbf{k}) = i\epsilon - \hat{\mathcal{H}}_0(\mathbf{k})$, where $\hat{\mathcal{H}}_0(\mathbf{k})$ is given by Eq. (4). We introduced a factor of $1/2$ in Eq. (48) to prevent the double counting of the electronic degrees of freedom since we use the four-component basis of Eq. (2).

To further elaborate on this aspect, we explore a concrete example for a nodal SC with two pairs of nodes. Specifically, we consider the $d = 2$ model with $v_\Delta > 0$:

$$\hat{\mathcal{H}}_0(\hat{\mathbf{p}}) = \tau_z \left(\frac{\hat{p}_y^2}{2m} - \alpha \hat{p}_y \sigma_z - \mu \right) + v_\Delta \hat{p}_x \tau_x \sigma_z, \quad (50)$$

which is obtained by means of dimensional reduction of the 3D model described in Eq. (41) to the 2D (x, y) plane, and harbors two pairs of nodal points located along the $k_x = 0$ high-symmetry line. The above model constitutes a paradigmatic model for the entire category of systems discussed here, since all nodes are situated along the same axis, thus allowing the generalization of some of our results to nodal SCs harboring multiple pair of nodes, with the various pairs of nodes been situated on lines with generally nonparallel orientation.

Before carrying out the calculation of the spin susceptibility, it is convenient to gauge away the SOC term by performing a spatially dependent unitary transformation:

$$\hat{\mathcal{H}}_0(\hat{\mathbf{p}}) = \mathcal{O}(y) \left(\frac{\hat{p}_y^2 - k_F^2}{2m} \tau_z + v_\Delta \hat{p}_x \tau_x \sigma_z \right) \mathcal{O}^\dagger(y), \quad (51)$$

with $k_F^2/(2m) = \mu + m\alpha^2/2$ and the kinetic energy term $\epsilon(k_y) = (k_y^2 - k_F^2)/(2m)$. Moreover, the unitary transformation matrix reads as $\mathcal{O}(y) = \text{Exp}(i\alpha y \sigma_z)$. Within this framework, the bare Green function in coordinate space becomes $\hat{G}_0(\epsilon, \mathbf{R}) = \mathcal{O}(Y) \hat{G}_0^{\alpha=0}(\epsilon, \mathbf{R})$, where we introduced

$\mathbf{R} = (X, Y)$, and the Green function for $\alpha = 0$:

$$\hat{G}_0^{\alpha=0}(\epsilon, \mathbf{R}) = \int \frac{d\mathbf{k}}{(2\pi)^2} e^{i\mathbf{k}\cdot\mathbf{R}} \frac{i\epsilon + \epsilon(k_y)\tau_z + v_\Delta k_x \tau_x \sigma_z}{(i\epsilon)^2 - (v_\Delta k_x)^2 - [\epsilon(k_y)]^2}. \quad (52)$$

We now proceed with the evaluation of the spin susceptibility. For this purpose, we also consider a semiclassical approach in which k_F is substantial, thus allowing to approximate the kinetic energy as $\epsilon(k_y) \approx \pm v_F(k_y \mp k_F)$, with the latter being expanded about the two Fermi points $k_y = \pm k_F$ with $v_F = k_F/m$. Moreover, due to the presence of the strong anisotropy, it is preferable to integrate over the k_x variable first. Since the integrand peaks at $k_x = 0$, we can safely consider that the integration is over $(-\infty, +\infty)$, without worrying about the possible necessity to introduce a cutoff. In this case, employing standard residue theory provides

$$\hat{G}_0^{\alpha=0}(\epsilon, \mathbf{R}) = - \int \frac{dk_y}{4\pi v_\Delta} e^{ik_y Y - \sqrt{[\epsilon(k_y)]^2 + \epsilon^2} |X|/v_\Delta} \times \left\{ \frac{i\epsilon + \epsilon(k_y)\tau_z}{\sqrt{[\epsilon(k_y)]^2 + \epsilon^2}} + i \text{sgn}(X) \tau_x \sigma_z \right\}. \quad (53)$$

By now exploiting the assumed semiclassical limit, we introduce the variable $\xi = \pm v_F(k_y \mp k_F)$ which allows us to carry out the substitution $k_y = \pm(k_F + \xi/v_F)$. After taking the limit $k_F \rightarrow \infty$, we obtain for $X, Y \neq 0$:

$$\hat{G}_0^{\alpha=0}(\epsilon, \mathbf{R}) = \frac{\cos(k_F Y)}{v_F v_\Delta} \int_{-\infty}^{+\infty} \frac{d\xi}{2\pi} e^{i\xi Y/v_F - \sqrt{\xi^2 + \epsilon^2} |X|/v_\Delta} \times \left\{ -\frac{i\epsilon}{\sqrt{\xi^2 + \epsilon^2}} - i \text{sgn}(X) \tau_x \sigma_z \right\} - \frac{\sin(k_F Y)}{v_\Delta} \times \frac{d}{dY} \int_{-\infty}^{+\infty} \frac{d\xi}{2\pi} \frac{e^{i\xi Y/v_F - \sqrt{\xi^2 + \epsilon^2} |X|/v_\Delta}}{\sqrt{\xi^2 + \epsilon^2}} \tau_z. \quad (54)$$

By further restricting to situations where $|X|$ is small with $\Theta = |X/Y| \ll 1$, we manage to obtain approximate closed-form expressions by replacing the exponential term $\text{Exp}(-\sqrt{\xi^2 + \epsilon^2} |X|/v_\Delta)$ by its factorized form $\text{Exp}(-|\xi| |X|/v_\Delta) \text{Exp}(-|\epsilon| |X|/v_\Delta)$ when evaluating the term $\propto \tau_x \sigma_z$, and by completely discarding it when evaluating the remaining two terms. These approximations lead to the expression

$$\pi v_F v_\Delta \hat{G}_0^{\alpha=0}(\epsilon, \mathbf{R}) \approx \sin(k_F |Y|) |\epsilon| K_1(|\epsilon| |Y|/v_F) \tau_z - \cos(k_F Y) \times \left[i\epsilon K_0(|\epsilon| |Y|/v_F) + \frac{iv_F^2 X e^{-|\epsilon| |X|/v_\Delta}}{v_\Delta Y^2} \tau_x \sigma_z \right]. \quad (55)$$

With the Green function at hand, we now determine the elements of the spin-susceptibility tensor. We find that for $\alpha = 0$, the only nonzero elements are $\chi_{xx}^{\alpha=0}(\mathbf{R}) = \chi_{yy}^{\alpha=0}(\mathbf{R}) \equiv \chi_{\text{in}}^{\alpha=0}(\mathbf{R}) = \mathcal{I}_1(\mathbf{R}) - \mathcal{I}_2(\mathbf{R}) + \mathcal{I}_3(\mathbf{R})$ and $\chi_{zz}^{\alpha=0}(\mathbf{R}) = \mathcal{I}_1(\mathbf{R}) - \mathcal{I}_2(\mathbf{R}) - \mathcal{I}_3(\mathbf{R})$, which consist of the three non-negative contributions presented below:

$$\mathcal{I}_1(\mathbf{R}) = \frac{1 + \cos(2k_F Y)}{2\pi (\pi v_\Delta Y)^2} \frac{v_F}{|Y|} \int_{-\infty}^{+\infty} du u^2 K_0^2(|u|), \quad (56)$$

$$\mathcal{I}_2(\mathbf{R}) = \frac{1 - \cos(2k_F Y)}{2\pi(\pi v_\Delta Y)^2} \frac{v_F}{|Y|} \int_{-\infty}^{+\infty} du u^2 K_1^2(|u|), \quad (57)$$

$$\mathcal{I}_3(\mathbf{R}) = \frac{\cos^2(k_F Y)}{\pi(\pi v_\Delta Y)^2} \frac{v_F}{|Y|} \frac{v_F}{v_\Delta} \Theta. \quad (58)$$

After the evaluation of $\int_{-\infty}^{+\infty} du u^2 K_0^2(|u|) = \pi^2/16$ and $\int_{-\infty}^{+\infty} du u^2 K_1^2(|u|) = 3\pi^2/16$, we find the following result:

$$\chi_{\text{in},zz}^{\alpha=0}(\mathbf{R}) \approx \frac{2 \cos(2k_F Y) - 1 \pm \Theta \frac{v_F}{v_\Delta} \left[\frac{4}{\pi} \cos(2k_F Y) \right]^2}{16\pi(v_\Delta Y)^2 |Y|/v_F}. \quad (59)$$

From the above, we conclude that when $\alpha = 0$ and two magnetic moments are placed along a line which is parallel to the y direction, the RKKY coupling is spin-isotropic since $\Theta = 0$. This is to be expected since, in this case, the $k_x = 0$ momentum is involved in the calculation of the Green function, which coincides with the line, along which, the pairs of nodes appear for the Hamiltonian of Eq. (50). From the Y dependence of the spin susceptibility, we find that both ferromagnetic (FM) and antiferromagnetic (AFM) solutions are accessible. In contrast, when the vector connecting the positions of two magnetic moments forms an angle with the y axis, then an easy plane/axis spin anisotropy sets in, and can be traced back to the spin-dependent p -wave pairing term in Eq. (50). For $\Theta \ll 1$, we find that when the distance between two moments is such so that it favors FM ordering, the spin anisotropy tends to align the magnetic moments in the plane, since in this case $\chi_{\text{in}}^{\alpha=0} > \chi_{zz}^{\alpha=0}$. On the other hand, for an intermoment distance favoring AFM ordering, the spin-anisotropy forces the magnetic moment to point out-of-the plane, i.e., along the z axis.

Let us now consider the effects of nonzero α which implies that the Rashba SOC is non-negligible. For a perfectly ordered array of localized magnetic moments with a spacing $|Y|$ in the y direction, we find that the z axis susceptibility is unaltered and the components $\chi_{xz,zy}$ remain zero. Nonetheless, there is now a modification of the strengths of the in plane susceptibilities. In addition to the above, the in-plane off diagonal elements $\chi_{xy}(\mathbf{R}) = -\chi_{yx}(\mathbf{R})$ become now nonzero. These results are reflected in the expressions

$$\chi_{\text{in}}(\mathbf{R}) = \cos(2m\alpha Y) \chi_{\text{in}}^{\alpha=0}(\mathbf{R}), \quad (60)$$

$$\chi_{xy}(\mathbf{R}) = \sin(2m\alpha Y) \chi_{\text{in}}^{\alpha=0}(\mathbf{R}). \quad (61)$$

Notably, a similar susceptibility structure has been discussed previously in Ref. [122] in connection to MZM platforms with magnetic chains. Here, the obtained spin-susceptibility transforms the emergent in plane FM order into an in-plane magnetic helix texture, while it leaves the out-plane AFM order unaffected. Since the z components of the magnetization become projected out in the low-energy model of Eq. (14) only the in-plane ordering of the magnetic moments can gap out the nodes. However, in the absence of additional sources of spin anisotropy, the arising FM-like magnetic helix texture cannot gap out the outer-helical branch nodes of the model in Eq. (50), since its winding compensates that of the Rashba SOC. A possible escapeway is to impose or engineer additional in-plane spin-anisotropies, which can allow to the magnetic moments to either develop in-plane

magnetic helix textures with a different pitch than the one characterizing the Rashba SOC, or enable in plane AFM phases.

For example the addition of terms such as $(S_n^x)^2$ generally opens the door for the above scenarios, as it has been already demonstrated in Ref. [122]. So far, we have not made any mentioning in connection to the pair of nodes associated with the inner helical branch arising due to the Rashba SOC. In analogy to Sec. VIII, also here, we can assume the presence of a weak Zeeman field in order to lift the inner helical branch [10,11]. Finally, we wish to remind the reader that the present platforms appear attractive for pinning MZMs in vortices of the arising in-plane magnetic helix texture or AFM order, since the spin-orientation of the magnetic moments is in principle locally tunable using scanning tunneling microscopy.

X. SUMMARY AND OUTLOOK

We provide a novel pathway to engineer Majorana zero modes (MZMs), which relies on nodal superconductors (SCs) and at the same time does not require the presence of superconducting vortices. In contrast, we show that MZMs become accessible in nodal SCs which are under the influence of magnetic texture crystals (MTCs). At this point, we wish to clarify that our approach is distinct to Refs. [48,125–129]. There, isolated magnetic skyrmions, and not crystals as we consider here, have been employed as smooth defects which pin various types of bound states in fully-gapped SCs, these including MZMs [48,126–128]. Instead, within our proposal, MZMs are pinned by spin and/or shift vortices induced in the MTC, which constitute singular defects.

Our analysis provides a detailed study of various topological scenarios in both 2D and 3D nodal SCs, which cover all three Majorana symmetry classes, i.e., BDI, D, and DIII. We present in detail the construction for two topological invariant quantities, which predict vortex MZMs in class BDI in 2D and chiral Majorana modes in class D in 3D. Topological invariants for the remaining cases can be constructed using these two fundamental invariants. Even more, we show how to render Majorana Kramers pair solutions still accessible, in spite of the violation of the standard time-reversal symmetry by the MTC. As an example we discuss a two-band model in 2D which harbors a single vortex Kramers pair of MZMs in 2D. Our analytical approach and predictions based on the various topological invariants are backed by our numerical simulations on the lattice.

The last part of our investigation concerns the experimental realization of our proposals in connection to intrinsic nodal SCs. We discuss the following three different possible paths to engineer the required MTCs and concomitant vortex MZMs: (i) MTCs which are engineered using nanomagnets, (ii) MTCs that arise spontaneously by virtue of the interactions dictating the electrons of the SC, and (iii) MTCs which are harbored by a lattice of localized magnetic moments which are exchange-coupled to the nodal SC. We provide insight in the above possibilities and discuss their advantages and possible limitations. Regarding the stabilization of vortices in MTCs, we note that certain types of topological defects in MTCs, e.g., disclinations [130,131], have already been experimentally observed in helimagnets [132–136]. Similarly,

shift/spin vortices can arise spontaneously, get pinned by disorder or engineered with nanomagnets, or scanning tunneling microscopy (STM) tips.

Apart from quantum materials, our idea may also be relevant for artificial platforms, such as a 2D electron gas (2DEG) in proximity to a conventional SC with strong Rashba SOC. Here, one wishes to harness the proximity effect to induce a mixed-spin type nodal pairing term in the 2DEG. This appears particularly promising for superconductor-semiconductor devices for which a strong debate has been raised recently [28,137–144]. We hope that our theory inspires the development of new platforms which take advantage of the advanced

fabrication and measurement techniques which currently exist for semiconductor hybrids, and combine them with the control over MTCs and vortex MZMs using spin-polarized STM.

ACKNOWLEDGMENTS

We thank M. H. Christensen and A. V. Balatsky for inspiring discussions. D.S. and B.M.A. acknowledge support from the Carlsberg Foundation, and P.K. from the National Natural Science Foundation of China (Grant No. 12050410262). B.M.A. additionally acknowledges support from the Independent Research Fund Denmark Grant No. 8021-00047B.

-
- [1] N. Read and D. Green, Paired states of fermions in two dimensions with breaking of parity and time-reversal symmetries, and the fractional quantum Hall effect, *Phys. Rev. B* **61**, 10267 (2000).
- [2] G. E. Volovik, Fermion zero modes on vortices in chiral superconductors, *JETP Lett.* **70**, 609 (1999).
- [3] D. A. Ivanov, Non-Abelian Statistics of Half-Quantum Vortices in P-Wave Superconductors, *Phys. Rev. Lett.* **86**, 268 (2001).
- [4] A. Y. Kitaev, Unpaired majorana fermions in quantum wires, *Phys. Usp.* **44**, 131 (2001).
- [5] Z. Wang, P. Zhang, G. Xu, L. K. Zeng, H. Miao, X. Xu, T. Qian, H. Weng, P. Richard, A. V. Fedorov, H. Ding, X. Dai, and Z. Fang, Topological nature of the FeSe_{0.5}Te_{0.5} superconductor, *Phys. Rev. B* **92**, 115119 (2015).
- [6] G. Xu, B. Lian, P. Tang, X.-L. Qi, and S.-C. Zhang, Topological Superconductivity on the Surface of Fe-Based Superconductors, *Phys. Rev. Lett.* **117**, 047001 (2016).
- [7] L. Fu and C. L. Kane, Superconducting Proximity Effect and Majorana Fermions at the Surface of a Topological Insulator, *Phys. Rev. Lett.* **100**, 096407 (2008).
- [8] J. D. Sau, R. M. Lutchyn, S. Tewari, and S. Das Sarma, Generic New Platform for Topological Quantum Computation Using Semiconductor Heterostructures, *Phys. Rev. Lett.* **104**, 040502 (2010).
- [9] J. Alicea, Majorana fermions in a tunable semiconductor device, *Phys. Rev. B* **81**, 125318 (2010).
- [10] R. M. Lutchyn, J. D. Sau, and S. Das Sarma, Majorana Fermions and a Topological Phase Transition in Semiconductor-Superconductor Heterostructures, *Phys. Rev. Lett.* **105**, 077001 (2010).
- [11] Y. Oreg, G. Refael, and F. von Oppen, Helical Liquids and Majorana Bound States in Quantum Wires, *Phys. Rev. Lett.* **105**, 177002 (2010).
- [12] R. S. K. Mong, D. J. Clarke, J. Alicea, N. H. Lindner, P. Fendley, C. Nayak, Y. Oreg, A. Stern, E. Berg, K. Shtengel, and M. P. A. Fisher, Universal Topological Quantum Computation from a Superconductor-Abelian Quantum Hall Heterostructure, *Phys. Rev. X* **4**, 011036 (2014).
- [13] A. Vaezi, Superconducting Analogue of the Parafermion Fractional Quantum Hall States, *Phys. Rev. X* **4**, 031009 (2014).
- [14] J. Klinovaja and D. Loss, Time-reversal invariant parafermions in interacting Rashba nanowires, *Phys. Rev. B* **90**, 045118 (2014).
- [15] M. Z. Hasan and C. L. Kane, Colloquium: Topological insulators, *Rev. Mod. Phys.* **82**, 3045 (2010).
- [16] X.-L. Qi and S.-C. Zhang, Topological insulators and superconductors, *Rev. Mod. Phys.* **83**, 1057 (2011).
- [17] A. Y. Kitaev, Fault-tolerant quantum computation by anyons, *Ann. Phys.* **303**, 2 (2003).
- [18] C. Nayak, S. H. Simon, A. Stern, M. Freedman, and S. Das Sarma, Non-Abelian anyons and topological quantum computation, *Rev. Mod. Phys.* **80**, 1083 (2008).
- [19] J. Alicea, Y. Oreg, G. Refael, F. von Oppen, and M. P. A. Fisher, Non-Abelian statistics and topological quantum information processing in 1D wire networks, *Nat. Phys.* **7**, 412 (2011).
- [20] J. Alicea, New directions in the pursuit of Majorana fermions in solid state systems, *Rep. Prog. Phys.* **75**, 076501 (2012).
- [21] C. W. J. Beenakker, Search for Majorana fermions in superconductors, *Annu. Rev. Condens. Matter Phys.* **4**, 113 (2013).
- [22] M. Leijnse and K. Flensberg, Introduction to topological superconductivity and Majorana fermions, *Semicond. Sci. Technol.* **27**, 124003 (2012).
- [23] S. R. Elliott and M. Franz, Colloquium: Majorana fermions in nuclear, particle, and solid-state physics, *Rev. Mod. Phys.* **87**, 137 (2015).
- [24] M. Sato and Y. Ando, Topological superconductors: A review, *Rep. Prog. Phys.* **80**, 076501 (2017).
- [25] R. Aguado, Majorana quasiparticles in condensed matter, *Riv. Nuovo Cim.* **40**, 523 (2017).
- [26] R. M. Lutchyn, E. P. A. M. Bakkers, L. P. Kouwenhoven, P. Krogstrup, C. M. Marcus, and Y. Oreg, Realizing Majorana zero modes in superconductor-semiconductor heterostructures, *Nat. Rev. Mater.* **3**, 52 (2018).
- [27] R. Pawlak, S. Hoffman, J. Klinovaja, D. Loss, and E. Meyer, Majorana fermions in magnetic chains, *Prog. Part. Nucl. Phys.* **107**, 1 (2019).
- [28] E. Prada, P. San-Jose, M. W. A. de Moor, A. Geresdi, E. J. H. Lee, J. Klinovaja, D. Loss, J. Nygård, R. Aguado, and L. P. Kouwenhoven, From andreev to majorana bound states in hybrid superconductor-semiconductor nanowires, *Nat. Rev. Phys.* **2**, 575 (2020).
- [29] V. Mourik, K. Zuo, S. M. Frolov, S. R. Plissard, E. P. A. M. Bakkers, and L. P. Kouwenhoven, Signatures of Majorana fermions in hybrid superconductor-semiconductor nanowire devices, *Science* **336**, 1003 (2012).

- [30] M. T. Deng, C. L. Yu, G. Y. Huang, M. Larsson, P. Caroff, and H. Q. Xu, Observation of Majorana fermions in a Nb-InSb Nanowire-Nb hybrid quantum device, *Nano Lett.* **12**, 6414 (2012).
- [31] A. Das, Y. Ronen, Y. Most, Y. Oreg, M. Heiblum, and H. Shtrikman, Evidence of majorana fermions in an Al - InAs nanowire topological superconductor, *Nat. Phys.* **8**, 887 (2012).
- [32] M. T. Deng, S. Vaitikienas, E. B. Hansen, J. Danon, M. Leijnse, K. Flensberg, P. Krogstrup, and C. M. Marcus, Majorana bound state in a coupled quantum-dot hybrid-nanowire system, *Science* **354**, 1557 (2016).
- [33] S. M. Albrecht, A. P. Higginbotham, M. Madsen, F. Kuemmeth, T. S. Jespersen, J. Nygård, P. Krogstrup, and C. M. Marcus, Exponential protection of zero modes in majorana islands, *Nature (London)* **531**, 206 (2016).
- [34] D. Laroche, D. Bouman, D. J. van Woerkom, A. Proutski, C. Murthy, D. I. Pikulin, C. Nayak, R. J. J. van Gulik, J. Nygård, P. Krogstrup, L. P. Kouwenhoven, and A. Geresdi, Observation of the 4π -periodic Josephson effect in indium arsenide nanowires, *Nat. Commun.* **10**, 245 (2019).
- [35] F. Nichele, A. C. C. Drachmann, A. M. Whiticar, E. C. T. O'Farrell, H. J. Suominen, A. Fornieri, T. Wang, G. C. Gardner, C. Thomas, A. T. Hatke, P. Krogstrup, M. J. Manfra, K. Flensberg, and C. M. Marcus, Scaling of Majorana Zero-Bias Conductance Peaks, *Phys. Rev. Lett.* **119**, 136803 (2017).
- [36] M. M. Desjardins, L. C. Contamin, M. R. Delbecq, M. C. Dartiailh, L. E. Bruhat, T. Cubaynes, J. J. Viennot, F. Mallet, S. Rohart, A. Thiaville, A. Cottet, T. Kontos, Synthetic spin orbit interaction for Majorana devices, *Nat. Mater.* **18**, 1060 (2019).
- [37] S. Manna, P. Wei, Y. Xie, K. T. Law, P. Lee, J. Moodera, Signature of a pair of Majorana zero modes in superconducting gold surface states, *Proc. Natl. Acad. Sci. U.S.A.* **117**, 8775 (2020).
- [38] S. Hart, H. Ren, T. Wagner, P. Leubner, M. Mühlbauer, C. Brüne, H. Buhmann, L. W. Molenkamp, and A. Yacoby, Induced superconductivity in the quantum spin hall edge, *Nat. Phys.* **10**, 638 (2014).
- [39] H.-H. Sun, K.-W. Zhang, L.-H. Hu, C. Li, G.-Y. Wang, H.-Y. Ma, Z.-A. Xu, C.-L. Gao, D.-D. Guan, Y.-Y. Li, C. Liu, D. Qian, Yi Zhou, L. Fu, S.-C. Li, F.-C. Zhang, and J.-F. Jia, Observation of majorana fermions with spin selective andreev reflection in the vortex of topological superconductor, *Phys. Rev. Lett.* **116**, 257003 (2016).
- [40] J. Wiedenmann, E. Bocquillon, R. S. Deacon, S. Hartinger, O. Herrmann, T. M. Klapwijk, L. Maier, C. Ames, C. Brüne, C. Gould, A. Oiwa, K. Ishibashi, S. Tarucha, H. Buhmann, and L. W. Molenkamp, 4π -periodic Josephson supercurrent in HgTe-based topological Josephson junctions, *Nat. Commun.* **7**, 10303 (2016).
- [41] L. Bours, B. Sothmann, M. Carrega, E. Strambini, E. M. Hankiewicz, L. W. Molenkamp, and F. Giazotto, A topological SQUIPT based on helical edge states in proximity to superconductors, *Phys. Rev. Appl.* **10**, 014027 (2018).
- [42] S. Nadj-Perge, I. K. Drozdov, Jian Li, Hua Chen, S. Jeon, J. Seo, A. H. MacDonald, B. A. Bernevig, and A. Yazdani, Observation of Majorana fermions in ferromagnetic atomic chains on a superconductor, *Science* **346**, 602 (2014).
- [43] M. Ruby, F. Pientka, Y. Peng, F. von Oppen, B. W. Heinrich, and K. J. Franke, End states and subgap structure in proximity-coupled chains of magnetic adatoms, *Phys. Rev. Lett.* **115**, 197204 (2015).
- [44] R. Pawlak, M. Kisiel, J. Klinovaja, T. Meier, S. Kawai, T. Glatzel, D. Loss, and E. Meyer, Probing atomic structure and Majorana wavefunctions in mono-atomic Fe-chains on superconducting Pb-surface, *npj Quantum Inf.* **2**, 16035 (2016).
- [45] S. Jeon, Y. Xie, J. Li, Z. Wang, B. A. Bernevig, and A. Yazdani, Distinguishing a Majorana zero mode using spin-resolved measurements, *Science* **358**, 772 (2017).
- [46] G. C. Ménard, S. Guissart, C. Brun, R. T. Leriche, M. Trif, F. Debontridder, D. Demaille, D. Roditchev, P. Simon, and T. Cren, Two-dimensional topological superconductivity in Pb/Co/Si(111), *Nat. Commun.* **8**, 2040 (2017).
- [47] H. Kim, A. Palacio-Morales, T. Posske, L. Rózsa, K. Palotás, L. Szunyogh, M. Thorwart, and R. Wiesendanger, Toward tailoring majorana bound states in artificially constructed magnetic atom chains on elemental superconductors, *Science Advances* **4**, eaar5251 (2018).
- [48] G. C. Ménard, A. Mesaros, C. Brun, F. Debontridder, D. Roditchev, P. Simon, and T. Cren, Isolated pairs of Majorana zero modes in a disordered superconducting lead monolayer, *Nat. Commun.* **10**, 2587 (2019).
- [49] G. C. Ménard, C. Brun, R. Leriche, M. Trif, F. Debontridder, D. Demaille, D. Roditchev, P. Simon, and T. Cren, Yu-Shiba-Rusinov bound states versus topological edge states in Pb/Si(111), *Eur. Phys. J. Spec. Top.* **227**, 2303 (2019).
- [50] J.-X. Yin, Zheng Wu, J.-H. Wang, Z.-Y. Ye, Jing Gong, X.-Y. Hou, Lei Shan, Ang Li, X.-J. Liang, X.-X. Wu, Jian Li, C.-S. Ting, Z. Wang, J.-P. Hu, P.-H. Hor, H. Ding, and S. H. Pan, Observation of a robust zero-energy bound state in iron-based superconductor Fe(Te, Se), *Nat. Phys.* **11**, 543 (2015).
- [51] P. Zhang, K. Yaji, T. Hashimoto, Y. Ota, T. Kondo, K. Okazaki, Z. Wang, J. Wen, G. D. Gu, H. Ding, and S. Shin, Observation of topological superconductivity on the surface of iron-based superconductor, *Science* **360**, 182 (2018).
- [52] D. Wang, L. Kong, P. Fan, H. Chen, S. Zhu, W. Liu, L. Cao, Y. Sun, S. Du, J. Schneeloch, R. Zhong, G. Gu, L. Fu, H. Ding, and H.-J. Gao, Observation of pristine Majorana bound state in iron-based superconductor, *Science* **362**, 333 (2018).
- [53] L. Kong, S. Zhu, M. Papaj, L. Cao, H. Isobe, W. Liu, D. Wang, P. Fan, H. Chen, Y. Sun, S. Du, J. Schneeloch, R. Zhong, G. Gu, L. Fu, H.-J. Gao, and H. Ding, Observation of half-integer level shift of vortex bound states in an iron-based superconductor, *Nat. Phys.* **15**, 1181 (2019).
- [54] S. Zhu, L. Kong, L. Cao, H. Chen, M. Papaj, S. Du, Y. Xing, W. Liu, D. Wang, C. Shen, F. Yang, J. Schneeloch, R. Zhong, G. Gu, L. Fu, Y.-Y. Zhang, H. Ding, and H.-J. Gao, Nearly quantized conductance plateau of vortex zero mode in an iron-based superconductor, *Science* **367**, 189 (2020).
- [55] G. E. Volovik, *The Universe in a Helium Droplet* (Oxford University Press, New York, 2003).
- [56] J. C. Y. Teo and C. L. Kane, Majorana Fermions and Non-Abelian Statistics in Three Dimensions, *Phys. Rev. Lett.* **104**, 046401 (2010).
- [57] M. Wimmer, A. R. Akhmerov, M. V. Medvedeva, J. Tworzdylo, and C. W. J. Beenakker, Majorana Bound States without Vortices in Topological Superconductors with Electrostatic Defects, *Phys. Rev. Lett.* **105**, 046803 (2010).

- [58] J. C. Y. Teo and C. L. Kane, Topological defects and gapless modes in insulators and superconductors, *Phys. Rev. B* **82**, 115120 (2010).
- [59] K. Shiozaki and M. Sato, Topology of crystalline insulators and superconductors, *Phys. Rev. B* **90**, 165114 (2014).
- [60] C. Chan, L. Zhang, T. F. J. Pooneffrey, Y.-P. He, Y.-Q. Wang, and X.-J. Liu, A Generic Theory for Majorana Zero Modes in 2D Superconductors, *Phys. Rev. Lett.* **119**, 047001 (2017).
- [61] M. Sato, Non-Abelian statistics of axion strings, *Phys. Lett. B* **575**, 126 (2003).
- [62] M. Sato, Y. Takahashi, and S. Fujimoto, Non-abelian topological order in s-wave superfluids of ultracold fermionic atoms, *Phys. Rev. Lett.* **103**, 020401 (2009).
- [63] A. P. Schnyder and P. M. R. Brydon, Topological surface states in nodal superconductors, *J. Phys.: Condens. Matter* **27**, 243201 (2015).
- [64] M. Kjaergaard, K. Wölms, and K. Flensberg, Majorana fermions in superconducting nanowires without spin-orbit coupling, *Phys. Rev. B* **85**, 020503(R) (2012).
- [65] I. Martin and A. F. Morpurgo, Majorana fermions in superconducting helical magnets, *Phys. Rev. B* **85**, 144505 (2012).
- [66] J. Klinovaja and D. Loss, Giant Spin-Orbit Interaction Due to Rotating Magnetic Fields in Graphene Nanoribbons, *Phys. Rev. X* **3**, 011008 (2013).
- [67] S. Nadj-Perge, I. K. Drozdov, B. A. Bernevig, and A. Yazdani, Proposal for realizing Majorana fermions in chains of magnetic atoms on a superconductor, *Phys. Rev. B* **88**, 020407(R) (2013).
- [68] P. Kotetes, Classification of engineered topological superconductors, *New J. Phys.* **15**, 105027 (2013).
- [69] S. Nakosai, Y. Tanaka, and N. Nagaosa, Two-dimensional p-wave superconducting states with magnetic moments on a conventional s-wave superconductor, *Phys. Rev. B* **88**, 180503(R) (2013).
- [70] B. Braunecker and P. Simon, Interplay between Classical Magnetic Moments and Superconductivity in Quantum One-Dimensional Conductors: Toward a Self-Sustained Topological Majorana Phase, *Phys. Rev. Lett.* **111**, 147202 (2013).
- [71] J. Klinovaja, P. Stano, A. Yazdani, and D. Loss, Topological Superconductivity and Majorana Fermions in RKKY Systems, *Phys. Rev. Lett.* **111**, 186805 (2013).
- [72] M. M. Vazifeh and M. Franz, Self-Organized Topological State with Majorana Fermions, *Phys. Rev. Lett.* **111**, 206802 (2013).
- [73] F. Pientka, L. I. Glazman, F. von Oppen, Topological superconducting phase in helical Shiba chains, *Phys. Rev. B* **88**, 155420 (2013).
- [74] K. Pöyhönen, A. Westström, J. Röntynen, and T. Ojanen, Majorana states in helical Shiba chains and ladders, *Phys. Rev. B* **89**, 115109 (2014).
- [75] N. Sedlmayr, J. M. Aguiar-Hualde, and C. Bena, Flat Majorana bands in 2D lattices with inhomogeneous magnetic fields: Topology and stability, *Phys. Rev. B* **91**, 115415 (2015).
- [76] D. Mandler, P. Kotetes, and G. Schön, Magnetic order on a topological insulator surface with warping and proximity-induced superconductivity, *Phys. Rev. B* **91**, 155405 (2015).
- [77] W. Chen and A. P. Schnyder, Majorana edge states in superconductor-noncollinear magnet interfaces, *Phys. Rev. B* **92**, 214502 (2015).
- [78] G. L. Fatin, A. Matos-Abiague, B. Scharf, and I. Žutić, Wireless Majorana Bound States: From Magnetic Tunability to Braiding, *Phys. Rev. Lett.* **117**, 077002 (2016).
- [79] M. Schechter, K. Flensberg, M. H. Christensen, B. M. Andersen, and J. Paaske, Self-organized topological superconductivity in a Yu-Shiba-Rusinov chain, *Phys. Rev. B* **93**, 140503(R) (2016).
- [80] M. H. Christensen, M. Schechter, K. Flensberg, B. M. Andersen and J. Paaske, Spiral magnetic order and topological superconductivity in a chain of magnetic adatoms on a 2D superconductor, *Phys. Rev. B* **94**, 144509 (2016).
- [81] P. Marra and M. Cuoco, Controlling Majorana states in topologically inhomogeneous superconductors, *Phys. Rev. B* **95**, 140504 (R) (2017).
- [82] T. Zhou, N. Mohanta, J. E. Han, A. Matos-Abiague, and I. Žutić, Tunable magnetic textures in spin valves: From spintronics to Majorana bound states, *Phys. Rev. B* **99**, 134505 (2019).
- [83] S. Rex, I. V. Gornyi, and A. D. Mirlin, Majorana modes in emergent-wire phases of helical and cycloidal magnet-superconductor hybrids, *Phys. Rev. B* **102**, 224501 (2020).
- [84] N. Mohanta, T. Zhou, J.-W. Xu, J. E. Han, A. D. Kent, J. Shabani, I. Žutić, and A. Matos-Abiague, Electrical Control of Majorana Bound States Using Magnetic Stripes, *Phys. Rev. Appl.* **12**, 034048 (2019).
- [85] G.-Y. Huang, B. Li, X.-F. Yi, J.-B. Fu, X. Fu, X.-G. Qiang, P. Xu, J.-J. Wu, C.-L. Yu, P. Kotetes, and M.-T. Deng, Field-Programmable Topological Array: Framework and Case-Studies, [arXiv:2010.02130](https://arxiv.org/abs/2010.02130).
- [86] L. P. Gor'kov and E. I. Rashba, Superconducting 2D System with Lifted Spin Degeneracy: Mixed Singlet-Triplet State, *Phys. Rev. Lett.* **87**, 037004 (2001).
- [87] A. Altland and M. R. Zirnbauer, Nonstandard symmetry classes in mesoscopic normal-superconducting hybrid structures, *Phys. Rev. B* **55**, 1142 (1997).
- [88] A. Kitaev, Periodic table for topological insulators and superconductors, in *Advances in Theoretical Physics: Landau Memorial Conference*, edited by V. Lebedev and M. Feigel'man, AIP Conf. Proc. No. 1134 (AIP, New York, 2009), p. 22.
- [89] S. Ryu, A. Schnyder, A. Furusaki and A. Ludwig, Topological insulators and superconductors: Ten-fold way and dimensional hierarchy, *New J. Phys.* **12**, 065010 (2010).
- [90] R. Jackiw and P. Rossi, Zero modes of the vortex-fermion system, *Nucl. Phys. B* **190**, 681 (1981).
- [91] Y. Nishida, L. Santos, and C. Chamon, Topological superconductors as nonrelativistic limits of Jackiw-Rossi and Jackiw-Rebbi models, *Phys. Rev. B* **82**, 144513 (2010).
- [92] M. Sigrist and K. Ueda, Phenomenological theory of unconventional superconductivity, *Rev. Mod. Phys.* **63**, 239 (1991).
- [93] E. Bauer, G. Hilscher, H. Michor, Ch. Paul, E. W. Scheidt, A. Gribanov, Yu. Seropegin, H. Noël, M. Sigrist, and P. Rogl, Heavy Fermion Superconductivity and Magnetic Order in Noncentrosymmetric CePt₃Si, *Phys. Rev. Lett.* **92**, 027003 (2004).
- [94] P. A. Frigeri, D. F. Agterberg, A. Koga, and M. Sigrist, Superconductivity without Inversion Symmetry: MnSi versus CePt₃Si, *Phys. Rev. Lett.* **92**, 097001 (2004).
- [95] M. Sato and S. Fujimoto, Topological phases of non-centrosymmetric superconductors: Edge states, majorana

- fermions, and the non-abelian statistics, *Phys. Rev. B* **79**, 094504 (2009).
- [96] M. Smidman, M. B. Salamon, H. Q. Yuan, and D. F. Agterberg, Superconductivity and spin-orbit coupling in non-centrosymmetric materials: A review, *Rep. Prog. Phys.* **80**, 036501 (2017).
- [97] C. de la Cruz, Q. Huang, J. W. Lynn, J. Li, W. Ratcliff, J. L. Zarestky, H. A. Mook, G. F. Chen, J. L. Luo, N. L. Wang, and P. Dai, Magnetic order close to superconductivity in the iron-based layered $\text{LaO}_{1-x}\text{F}_x\text{FeAs}$ systems, *Nature (London)* **453**, 899 (2008).
- [98] C. Liu, T. Kondo, R. M. Fernandes, A. D. Palczewski, E. D. Mun, N. Ni, A. N. Thaler, A. Bostwick, E. Rotenberg, J. Schmalian, S. L. Bud'ko, P. C. Canfield, and A. Kaminski, Evidence for a Lifshitz transition in electron-doped iron arsenic superconductors at the onset of superconductivity, *Nat. Phys.* **6**, 419 (2010).
- [99] M. J. A. Jardine, J. P. T. Stenger, Y. Jiang, E. J. de Jong, W. Wang, A. C. B. Jayich, and S. M. Frolov, Integrating micromagnets and hybrid nanowires for topological quantum computing, [arXiv:2104.05130](https://arxiv.org/abs/2104.05130).
- [100] A. A. El-Gendy, M. Bertino, D. Clifford, M. Qian, S. N. Khanna, and E. E. Carpenter, Experimental evidence for the formation of CoFe_2C phase with colossal magnetocrystalline-anisotropy, *Appl. Phys. Lett.* **106**, 213109 (2015).
- [101] G. Grüner, The dynamics of spin-density waves, *Rev. Mod. Phys.* **66**, 1 (1994).
- [102] S. Avci, O. Chmaissem, J. M. Allred, S. Rosenkranz, I. Eremin, A. V. Chubukov, D. E. Bugaris, D. Y. Chung, M. G. Kanatzidis, J.-P. Castellán, J. A. Schlueter, H. Claus, D. D. Khalyavin, P. Manuel, A. Daoud-Aladine, and R. Osborn, Magnetically driven suppression of nematic order in an iron-based superconductor, *Nat. Commun.* **5**, 3845 (2014).
- [103] F. Waßer, A. Schneidewind, Y. Sidis, S. Wurmehl, S. Aswartham, B. Büchner, and M. Braden, Spin reorientation in $\text{Ba}_{0.65}\text{Na}_{0.35}\text{Fe}_2\text{As}_2$ studied by single-crystal neutron diffraction, *Phys. Rev. B* **91**, 060505 (2015).
- [104] E. Hassinger, G. Gredat, F. Valade, S. R. de Cotret, A. Juneau-Fecteau, J.-P. Reid, H. Kim, M. A. Tanatar, R. Prozorov, B. Shen, H.-H. Wen, N. Doiron-Leyraud, and L. Taillefer, Pressure-induced Fermi-surface reconstruction in the iron-arsenide superconductor $\text{Ba}_{1-x}\text{K}_x\text{Fe}_2\text{As}_2$: Evidence of a phase transition inside the antiferromagnetic phase, *Phys. Rev. B* **86**, 140502 (2012).
- [105] A. E. Böhmer, F. Hardy, L. Wang, T. Wolf, P. Schweiss, and C. Meingast, Superconductivity-induced re-entrance of the orthorhombic distortion in $\text{Ba}_{1-x}\text{K}_x\text{Fe}_2\text{As}_2$, *Nat. Commun.* **6**, 7911 (2015).
- [106] J. M. Allred, S. Avci, Y. Chung, H. Claus, D. D. Khalyavin, P. Manuel, K. M. Taddei, M. G. Kanatzidis, S. Rosenkranz, R. Osborn, and O. Chmaissem, Tetragonal magnetic phase in $\text{Ba}_{1-x}\text{K}_x\text{Fe}_2\text{As}_2$ from x-ray and neutron diffraction, *Phys. Rev. B* **92**, 094515 (2015).
- [107] Y. Zheng, P. M. Tam, J. Hou, A. E. Böhmer, T. Wolf, C. Meingast, and R. Lortz, Absence of nematic order in the pressure-induced intermediate phase of the iron-based superconductor $\text{Ba}_{0.85}\text{K}_{0.15}\text{Fe}_2\text{As}_2$, *Phys. Rev. B* **93**, 104516 (2016).
- [108] B. P. P. Mallett, Y. G. Pashkevich, A. Gusev, T. Wolf, and C. Bernhard, Muon spin rotation study of the magnetic structure in the tetragonal antiferromagnetic state of weakly underdoped $\text{Ba}_{1-x}\text{K}_x\text{Fe}_2\text{As}_2$, *Europhys. Lett.* **111**, 57001 (2015).
- [109] B. P. P. Mallett, P. Marsik, M. Yazdi-Rizi, T. Wolf, A. E. Böhmer, F. Hardy, C. Meingast, D. Munzar, and C. Bernhard, Infrared Study of the Spin Reorientation Transition and Its Reversal in the Superconducting State in Underdoped $\text{Ba}_{1-x}\text{K}_x\text{Fe}_2\text{As}_2$, *Phys. Rev. Lett.* **115**, 027003 (2015).
- [110] D. K. Pratt, M. G. Kim, A. Kreyssig, Y. B. Lee, G. S. Tucker, A. Thaler, W. Tian, J. L. Zarestky, S. L. Budko, P. C. Canfield, B. N. Harmon, A. I. Goldman, and R. J. McQueeney, Incommensurate Spin-Density Wave Order in Electron-Doped BaFe_2As_2 Superconductors, *Phys. Rev. Lett.* **106**, 257001 (2011).
- [111] J. M. Allred, K. M. Taddei, D. E. Bugaris, M. J. Krogstad, S. H. Lapidus, D. Y. Chung, H. Claus, M. G. Kanatzidis, D. E. Brown, J. Kang, R. M. Fernandes, I. Eremin, S. Rosenkranz, O. Chmaissem, and R. Osborn, Double-Q spin-density wave in iron arsenide superconductors, *Nat. Phys.* **12**, 493 (2016).
- [112] W. R. Meier, Q.-P. Ding, A. Kreyssig, S. L. Bud'ko, A. Sapkota, K. Kothapalli, V. Borisov, R. Valentí, C. D. Batista, P. P. Orth, R. M. Fernandes, A. I. Goldman, Y. Furukawa, A. E. Böhmer, and P. C. Canfield, Hedgehog spin-vortex crystal stabilized in a hole-doped iron-based superconductor, *npj Quant. Mat.* **3**, 5 (2018).
- [113] L. Wang, F. Hardy, A. E. Böhmer, T. Wolf, P. Schweiss, and C. Meingast, Complex phase diagram of $\text{Ba}_{1-x}\text{Na}_x\text{Fe}_2\text{As}_2$: A multitude of phases striving for the electronic entropy, *Phys. Rev. B* **93**, 014514 (2016).
- [114] E. Wiesenmayer, H. Luetkens, G. Pascua, R. Khasanov, A. Amato, H. Potts, B. Banusch, H.-H. Klauss, and D. Johrendt, Microscopic Coexistence of Superconductivity and Magnetism in $\text{Ba}_{1-x}\text{K}_x\text{Fe}_2\text{As}_2$, *Phys. Rev. Lett.* **107**, 237001 (2011).
- [115] S. Avci, O. Chmaissem, E. A. Goremychkin, S. Rosenkranz, J.-P. Castellán, D. Y. Chung, I. S. Todorov, J. A. Schlueter, H. Claus, M. G. Kanatzidis, A. Daoud-Aladine, D. Khalyavin, and R. Osborn, Magnetoelastic coupling in the phase diagram of $\text{Ba}_{1-x}\text{K}_x\text{Fe}_2\text{As}_2$ as seen via neutron diffraction, *Phys. Rev. B* **83**, 172503 (2011).
- [116] P. Materne, S. Kamusella, R. Sarkar, T. Goltz, J. Spehling, H. Maeter, L. Harnagea, S. Wurmehl, B. Büchner, H. Luetkens, C. Timm, and H.-H. Klauss, Coexistence of superconductivity and magnetism in $\text{Ca}_{1-x}\text{Na}_x\text{Fe}_2\text{As}_2$: Universal suppression of the magnetic order parameter in 122 iron pnictides, *Phys. Rev. B* **92**, 134511 (2015).
- [117] N. Ni, M. E. Tillman, J.-Q. Yan, A. Kracher, S. T. Hannahs, S. L. Bud'ko, and P. C. Canfield, Effects of Co substitution on thermodynamic and transport properties and anisotropic H_{c2} in $\text{Ba}(\text{Fe}_{1-x}\text{Co}_x)_2\text{As}_2$ single crystals, *Phys. Rev. B* **78**, 214515 (2008).
- [118] S. Nandi, M. G. Kim, A. Kreyssig, R. M. Fernandes, D. K. Pratt, A. Thaler, N. Ni, S. L. Bud'ko, P. C. Canfield, J. Schmalian, R. J. McQueeney, and A. I. Goldman, Anomalous Suppression of the Orthorhombic Lattice Distortion in Superconducting $\text{Ba}(\text{Fe}_{1-x}\text{Co}_x)_2\text{As}_2$ Single Crystals, *Phys. Rev. Lett.* **104**, 057006 (2010).
- [119] M. H. Christensen, B. M. Andersen, and P. Kotetes, Unravelling Incommensurate Magnetism and its Emergence in Iron-Based Superconductors, *Phys. Rev. X* **8**, 041022 (2018).

- [120] P. M. R. Brydon, H.-Y. Hui, and J. D. Sau, Topological Yu-Shiba-Rusinov chain from spin-orbit coupling, *Phys. Rev. B* **91**, 064505 (2015).
- [121] J. Li, H. Chen, I. K. Drozdov, A. Yazdani, B. A. Bernevig, and A. H. MacDonald, Topological superconductivity induced by ferromagnetic metal chains, *Phys. Rev. B* **90**, 235433 (2014).
- [122] A. Heimes, D. Mendler, and P. Kotetes, Interplay of topological phases in magnetic adatom-chains on top of a rashba superconducting surface, *New J. Phys.* **17**, 023051 (2015).
- [123] P. Kotetes, D. Mendler, A. Heimes, and G. Schön, Majorana fermion fingerprints in spin-polarised scanning tunneling microscopy, *Phys. E* **74**, 614 (2015).
- [124] S. Doniach, The Kondo lattice and weak antiferromagnetism, *Physica B+C* **91**, 231 (1977).
- [125] S. S. Pershoguba, S. Nakosai, and A. V. Balatsky, Skyrmion-induced bound states in a superconductor, *Phys. Rev. B* **94**, 064513 (2016).
- [126] G. Yang, P. Stano, J. Klinovaja, and D. Loss, Majorana bound states in magnetic skyrmions, *Phys. Rev. B* **93**, 224505 (2016).
- [127] S. Rex, I. V. Gornyi, and A. D. Mirlin, Majorana bound states in magnetic skyrmions imposed onto a superconductor, *Phys. Rev. B* **100**, 064504 (2019).
- [128] M. Garnier, A. Mesaros, and P. Simon, Topological superconductivity with orbital effects in magnetic skyrmion based heterostructures, [arXiv:1909.12671](https://arxiv.org/abs/1909.12671).
- [129] M. Garnier, A. Mesaros, and P. Simon, Topological superconductivity with deformable magnetic skyrmions, *Commun. Phys.* **2**, 126 (2019).
- [130] Fuxiang Li, T. Nattermann, and V. L. Pokrovsky, Vortex Domain Walls in Helical Magnets, *Phys. Rev. Lett.* **108**, 107203 (2012).
- [131] T. Nattermann and V. L. Pokrovsky, Topological defects in helical magnets, *J. Exp. Theor. Phys.* **127**, 922 (2018).
- [132] M. Uchida, N. Nagaosa, J. P. He, Y. Kaneko, S. Iguchi, Y. Matsui, and Y. Tokura, Topological spin textures in the helimagnet FeGe, *Phys. Rev. B* **77**, 184402 (2008).
- [133] P. Milde, D. Köhler, J. Seidel, L. M. Eng, A. Bauer, A. Chacon, J. Kindervater, S. Mühlbauer, C. Pfleiderer, S. Buhrandt, C. Schütte, and A. Rosch, Unwinding of a skyrmion lattice by magnetic monopoles, *Science* **340**, 1076 (2013).
- [134] A. Dussaux, P. Schoenherr, K. Koumpouras, J. Chico, K. Chang, L. Lorenzelli, N. Kanazawa, Y. Tokura, M. Garst, A. Bergman, C. L. Degen, and D. Meier, Local dynamics of topological magnetic defects in the itinerant helimagnet FeGe, *Nat. Commun.* **7**, 12430 (2016).
- [135] A. Bauer, A. Chacon, M. Wagner, M. Halder, R. Georgii, A. Rosch, C. Pfleiderer, and M. Garst, Symmetry breaking, slow relaxation dynamics, and topological defects at the field-induced helix reorientation in MnSi, *Phys. Rev. B* **95**, 024429 (2017).
- [136] P. Schoenherr, J. Müller, L. Köhler, A. Rosch, N. Kanazawa, Y. Tokura, M. Garst, and D. Meier, Topological domain walls in helimagnets, *Nat. Phys.* **14**, 465 (2018).
- [137] C.-X. Liu, J. D. Sau, T. D. Stanescu, and S. Das Sarma, Andreev bound states versus majorana bound states in quantum dot-nanowire-superconductor hybrid structures: Trivial versus topological zero-bias conductance peaks, *Phys. Rev. B* **96**, 075161 (2017).
- [138] C. Moore, T. D. Stanescu, and S. Tewari, Two-terminal charge tunneling: Disentangling majorana zero modes from partially separated andreev bound states in semiconductor-superconductor heterostructures, *Phys. Rev. B* **97**, 165302 (2018).
- [139] C. Reeg, O. Dmytruk, D. Chevallerier, D. Loss, and J. Klinovaja, Zero-energy andreev bound states from quantum dots in proximitized rashba nanowires, *Phys. Rev. B* **98**, 245407 (2018).
- [140] B. D. Woods, J. Chen, S. M. Frolov, and T. D. Stanescu, Zero-energy pinning of topologically trivial bound states in multiband semiconductor-superconductor nanowires, *Phys. Rev. B* **100**, 125407 (2019).
- [141] J. Chen, B. Woods, P. Yu, M. Hoeschele, D. Car, S. Plissard, E. Bakkers, T. Stanescu, and S. Frolov, Ubiquitous non-Majorana Zero-Bias Conductance Peaks in Nanowire Devices, *Phys. Rev. Lett.* **123**, 107703 (2019).
- [142] A. Vuik, B. Nijholt, A. R. Akhmerov, and M. Wimmer, Reproducing topological properties with quasi-Majorana states, *SciPost Phys.* **7**, 061 (2019).
- [143] H. Pan and S. Das Sarma, Physical mechanisms for zero-bias conductance peaks in Majorana nanowires, *Phys. Rev. Res.* **2**, 013377 (2020).
- [144] P. Yu, J. Chen, M. Gomanko, G. Badawy, E. P. A. M. Bakkers, K. Zuo, V. Mourik, and S. M. Frolov, Non-Majorana states yield nearly quantized conductance in proximatized nanowires, *Nat. Phys.* **17**, 482 (2021).